Chinese Physics C

PAPER • OPEN ACCESS

One-loop contributions for $h \to \ell\bar{\ell}\gamma$ and $e^-e^+ \to h\gamma$ in the $U(1)_{B-L}$ extension of the standard model*

To cite this article: Tran Dzung Tri *et al* 2024 *Chinese Phys. C* **48** 053101

One-loop contributions for $h \to \ell\bar{\ell}\gamma$ and $e^-e^+ \to h\gamma$ in the $U(1)_{B-L}$ extension of the standard model*

Tran Dzung Tri[a,b] Thanh Huy Nguyen[c] Khiem Hong Phan[a,b†]

[a]Institute of Fundamental and Applied Sciences, Duy Tan University, Ho Chi Minh City 700000, Vietnam
[b]Faculty of Natural Sciences, Duy Tan University, Da Nang City 550000, Vietnam
[c]VNUHCM-University of Science, 227 Nguyen Van Cu, District 5, Ho Chi Minh City, Vietnam

Abstract: We present one-loop contributions for $h \to \ell\bar{\ell}\gamma$ with $\ell = \nu_{e,\mu,\tau}, e, \mu$ and $e^-e^+ \to h\gamma$ in the $U(1)_{B-L}$ extension of the standard model. In the phenomenological results, the signal strengths for $h \to \ell\bar{\ell}\gamma$ at the Large Hadron Collider and for $e^-e^+ \to h\gamma$ at future lepton colliders are analyzed in the physical parameter space for both the vector and chiral $B-L$ models. We found that the contributions from the neutral gauge boson Z' to the signal strengths are rather small. Consequently, the effects will be difficult to probe at future colliders. However, the impacts of charged Higgs and CP-odd Higgs in the chiral $B-L$ model on the signal strengths are significant and can be measured with the help of the initial polarization beams at future lepton colliders.

Keywords: Higgs phenomenology, one-loop Feynman integrals, analytic methods for quantum field theory, dimensional regularization, future lepton colliders

DOI: 10.1088/1674-1137/ad2441

I. INTRODUCTION

The precise measurements of the decay rates and production cross-sections of the standard-model-like Higgs boson (SM-like Higgs boson) h are primary targets at the High-Luminosity Large Hadron Collider (HL-LHC) [1, 2] as well as future lepton colliders (LCs) [3]. From the measured data, we can probe accurately the properties of the SM-like Higgs boson. In this perspective, the nature of the scalar Higgs potential can be discovered. In other words, we can deeply understand the electroweak spontaneous symmetry breaking (EWSB). The updated measurements for the Higgs boson production cross-sections and decay rates at ATLAS and CMS can be found in Refs. [4, 5] and the references therein. Moreover, the loop-induced processes $h \to \gamma\gamma$ and $h \to Z\gamma$ have been measured at the LHC [6–12]. More recently, the decay processes $h \to \ell\bar{\ell}\gamma$ with $\ell = \nu_{e,\mu,\tau}, e, \mu$ have also received significant attention at the LHC [13–16]. Together with $h \to \gamma\gamma, Z\gamma$, the decay processes $h \to \ell\bar{\ell}\gamma$ provide important information for testing the standard model (SM) [17–19] and the constraining parameters in many of beyond the standard models (BSMs) [19].

One-loop contributions for the decay processes $h \to \ell\bar{\ell}\gamma$ have been performed in Refs. [20–27] in the SM. In the framework of the two Higgs doublet models (THDM), one-loop decay processes $h \to \ell\bar{\ell}\gamma$ have been evaluated in Refs. [28, 29]. Recently, one-loop expressions for $h \to \ell\bar{\ell}\gamma$ in general BSM frameworks have been presented in Refs. [30, 31]. We have derived alternative presentations for one-loop contributions of $h \to \ell\bar{\ell}\gamma$ in the Higgs extension of the standard model (HESM) [32]. In [32], the computations have addressed the 't Hooft-Feynman (HF) gauge and confirm the results in our previous studies [30, 31] in the unitary gauge. We note that all contributions of singly and doubly charged Higgses propagating in the loop diagrams have been taken into account in Ref. [32]. It is well-known that there also exist many new gauge bosons exchanging in the loop diagrams of the decay processes $h \to \ell\bar{\ell}\gamma$ in other BSMs. For example, in the simplest $U(1)_{B-L}$ extension for the SM [33–42], a neutral Z' gauge boson exists. In the left-right models (LR) constructed from the $SU(2)_L \times SU(2)_R \times U(1)_Y$ [43–45], 3-3-1 models ($SU(3)_L \times U(1)_X$) [46–52], 3-4-1 models ($SU(4)_L \times U(1)_X$) [52–57], *etc.*, new charged gauge bosons as well as new neutral gauge bosons are included. Therefore, one-loop formulas for the decay rates of $h \to \ell\bar{\ell}\gamma$ in the above-mentioned models are of great

Received 10 November 2023; Accepted 31 January 2024; Published online 1 February 2024

* Supported by Vietnam National Foundation for Science and Technology Development (NAFOSTED, 103.01-2023.16)

† E-mail: phanhongkhiem@duytan.edu.vn

interest. The calculations for $h\to\ell\bar{\ell}\gamma$ in the HF gauge have several advantages as discussed in [32]. It is difficult to derive general one-loop formulas for $h\to\ell\bar{\ell}\gamma$ in the HF gauge for the arbitrary BSM as we have performed in [31]. Because of the couplings of new particles to Goldstone bosons, ghost particles depend on the models under consideration. Owing to gauge invariance, the contribution from Goldstone bosons, ghost particles propagating in the loop will be cancelled out at the final results. The cancellations within the vector boson loop with their Goldstone bosons. The ghost particles exchanging in the loop may not be the same in the different BSMs. For this reason, in this work, we compute the one-loop contribution for $h\to\ell\bar{\ell}\gamma$ with $\ell=\nu_{e,\mu,\tau},e,\mu$ and $e^-e^+\to h\gamma$ in the $U(1)_{B-L}$ extension of the SM in the HF gauge. In comparison with the work in [31], we present alternative expressions for the one-loop contribution for $h\to\ell\bar{\ell}\gamma$ in the HF gauge within the $U(1)_{B-L}$ models. This work also extends the results in [32] by adding the new contributions of the neutral gauge boson Z' as well as heavy neutrinos in the models.

In another aspect, the couplings of the Higgs boson with $Z\gamma,\gamma\gamma$ can be probed by measuring the cross-sections of the Higgs boson production associated with a photon at future LCs. It is important to note that the tree-level cross-section for this process is proportional to the electron mass, and the process follows the electromagnetic gauge symmetry. Therefore, it is a significant contribution from the one-loop level. As a result, the cross-section is rather small because, compared with the LHC, the LC has a cleaner background. The new physic signals are thus easily extracted from the background. With the high-luminosity designed at future LCs [3], the signal of Higgs boson production associated with a photon can be probed. Many computations for one-loop corrections to $e^-e^+\to h\gamma$ at future LCs in the SM are available [58–60], such as those in many frameworks of the HESM [61–63] and in the minimal supersymmetric standard model [64]. In this work, we show that cross-sections of $e^-e^+\to h\gamma$ can be derived by using one-loop form factors in $h\to\ell\bar{\ell}\gamma$. The results are also valid in the SM, within the $U(1)_{B-L}$ extension of the standard model, and can be extended to other BSMs.

In the phenomenological studies, we present the first results of analyzing the signal strengths for $h\to\ell\bar{\ell}\gamma$ at the LHC and for $e^-e^+\to h\gamma$ at future LCs in the physical parameter space for both vector and chiral $B-L$ models. For the decay processes $h\to\ell\bar{\ell}\gamma$, we focus on the possibility to probe the heavy neutral gauge boson Z' as well as the charged Higgs and CP-odd Higgs at the LHC. For this reason, we are interested in the case of heavy neutrinos scenario ($M_{N_i}\sim$ TeV). For the production process $e^-e^+\to h\gamma$ at future LCs, the signal strengths are examined by including the initial beam polarization effects. The contributions of the neutral gauge boson Z', charged Higgs, CP-odd Higgs, as well as additional neutrinos are investigated in further detail at future LCs.

Our work is organized as follows. In Sec. II, the $U(1)_{B-L}$ extension of the SM is reviewed in more detail. In Sec. III, we present the concrete evaluations for one-loop form factors for the decay channels $h\to\ell\bar{\ell}\gamma$ and for the process $e^-e^+\to h\gamma$. The phenomenological results for the processes are discussed in Sec. IV. The conclusions and outlook are included in Sec. V. In the appendices, we calculate all the couplings related to the processes under consideration.

II. REVIEW OF $U(1)_{B-L}$ EXTENSION OF THE STANDARD MODEL

In this section, following [33], we review in detail the $U(1)_{B-L}$ model, one of the simplest extensions of the SM. The model enlarges the SM gauge group with a new gauge symmetry $U(1)_{B-L}$. The $U(1)_{B-L}$ extension model then follows the gauge group $SU(3)_C\otimes SU(2)_L\otimes U(1)_Y\otimes U(1)_{B-L}$. As a result, the Yang-Mills Lagrangian including the mixing of two $U(1)$ abelian gauge groups is modified as follows:

$$\mathcal{L}_{YM}=-\frac{1}{4}G^{a,\mu\nu}G_{a,\mu\nu}-\frac{1}{4}W^{a,\mu\nu}W_{a,\mu\nu}-\frac{1}{4}B^{\mu\nu}B_{\mu\nu}-\frac{1}{4}X^{\mu\nu}X_{\mu\nu}-\frac{\kappa}{2}B^{\mu\nu}X_{\mu\nu} \tag{1}$$

where $G^{a,\mu\nu}$, $W^{a,\mu\nu}$ correspond to the field strengths of the gauge groups $SU(3)_C,SU(2)_L$, whereas $B_{\mu\nu}$ and $X_{\mu\nu}$ are the field strengths of the gauge groups $U(1)_Y$ and $U(1)_{B-L}$, respectively. Considering the mixing term (kinematic mixing case), we have to perform the following rotation for two gauge bosons in the groups of $U(1)_Y$, $U(1)_{B-L}$:

$$\begin{pmatrix}\tilde{B}_\mu\\ \tilde{X}_\mu\end{pmatrix}=\begin{pmatrix}1 & \kappa\\ 0 & \sqrt{1-\kappa^2}\end{pmatrix}\begin{pmatrix}B_\mu\\ X_\mu\end{pmatrix}. \tag{2}$$

Here, κ is the mixing parameter between the gauge groups $U(1)_Y$ and $U(1)_{B-L}$. We note that g,g' (g_X) are the couplings of the $SU(2)_L,U(1)_Y$, ($U(1)_{B-L}$) gauge groups, respectively. In this paper, we note the hypercharge Y for the $U(1)_Y$ gauge group and Y_X for the $U(1)_{B-L}$ gauge group. The model is classified into two types of models, the vector $B-L$ model and the chiral $B-L$ model [33]. These models are studied in further detail in the following subsections.

A. Vector $B-L$ model

In the vector $B-L$ model, we have three additional right handed neutrinos (RHNs, N_i for $i=\overline{1,2,3}$) and a new complex scalar singlet field χ, which is required for

the spontaneous symmetry breaking (SSB) of the $U(1)_{B-L}$ gauge. In this version, the matter fields, scalar fields are listed with their quantum numbers in the following Table 1.

The Higgs sector is given by

$$\mathcal{L}_H = \mathcal{L}_K - \mathcal{V}(\Phi,\chi). \tag{3}$$

Here, the kinematic part reads as

$$\mathcal{L}_K = (D_\mu\Phi)^\dagger D_\mu\Phi + (D^\mu\chi)^\dagger D^\mu\chi \tag{4}$$

and the scalar potential $\mathcal{V}(\Phi,\chi)$ is given by

$$\mathcal{V}(\Phi,\chi) = m_\chi^2(\chi^*\chi) + \frac{1}{2}\lambda_\chi(\chi^*\chi)^2 + m_\Phi^2(\Phi^\dagger\Phi) + \frac{1}{2}\lambda_\Phi(\Phi^\dagger\Phi)^2 + \lambda_{\Phi\chi}(\chi^*\chi)(\Phi^\dagger\Phi). \tag{5}$$

The fields Φ and χ are parameterized for spontaneous symmetry breaking as follows:

$$\Phi = \frac{1}{\sqrt{2}}\begin{pmatrix} \sqrt{2}G^\pm \\ v_\Phi + R_1 + \mathrm{i}I_1 \end{pmatrix}, \quad \chi = \frac{1}{\sqrt{2}}(v_\chi + R_2 + \mathrm{i}I_2). \tag{6}$$

Here, the Goldstone bosons $G^\pm$ are giving the masses for the $W^\pm$ bosons, whereas the I_1, I_2 fields are mixed together, being neutral Goldstone bosons $G^0_{1,2}$. They play a role for giving masses to the gauge bosons Z and Z', respectively. The minimization for the scalar potential leads to a system of equations as follows:

$$m_\chi^2 + \frac{\lambda_\chi}{2}v_\chi^2 + \frac{\lambda_{\Phi\chi}}{2}v_\Phi^2 = 0, \tag{7}$$

$$m_\Phi^2 + \frac{\lambda_\Phi}{2}v_\Phi^2 + \frac{\lambda_{\Phi\chi}}{2}v_\chi^2 = 0. \tag{8}$$

From the minimization conditions for $\mathcal{V}(\Phi,\chi)$, one can present m_χ^2, m_Φ^2 in terms of the remaining parameters in the potential. As a result, the mass matrix for the neutral scalar components is collected on the basis of (R_1, R_2) as follows:

$$\mathcal{M}_S^2 = \begin{pmatrix} v_\Phi^2\lambda_\Phi v_\Phi v_\chi\lambda_{\Phi\chi} \\ v_\Phi v_\chi\lambda_{\Phi\chi} v_\chi^2\lambda_\chi \end{pmatrix}. \tag{9}$$

To diagonalize the matrix in Eq. (9) for obtaining the Higgs physical masses of neutral Higgses, one first performs the rotation that shows the relation of (h, H) and (R_1, R_2). The rotation matrix takes the form of

$$\begin{pmatrix} h \\ H \end{pmatrix} = \begin{pmatrix} c_\theta & -s_\theta \\ s_\theta & c_\theta \end{pmatrix}\begin{pmatrix} R_1 \\ R_2 \end{pmatrix} \tag{10}$$

with mixing angle

$$t_{2\theta} = \frac{2\lambda_{\Phi\chi}v_\Phi v_\chi}{\lambda_\chi v_\chi^2 - \lambda_\Phi v_\Phi^2}. \tag{11}$$

The masses of the CP-even Higgs scalars take then the form of

$$M_h^2 = \frac{1}{2}[v_\Phi^2\lambda_\Phi + v_\chi^2\lambda_\chi - \sqrt{(v_\Phi^2\lambda_\Phi - v_\chi^2\lambda_\chi)^2 + 4v_\Phi^2 v_\chi^2\lambda_{\Phi\chi}^2}], \tag{12}$$

$$M_H^2 = \frac{1}{2}[v_\Phi^2\lambda_\Phi + v_\chi^2\lambda_\chi + \sqrt{(v_\Phi^2\lambda_\Phi - v_\chi^2\lambda_\chi)^2 + 4v_\Phi^2 v_\chi^2\lambda_{\Phi\chi}^2}]. \tag{13}$$

In this work, we assume that $M_h^2 \le M_H^2$, h being the SM-like Higgs boson with $M_h \sim 125$ GeV.

From the kinematic term of the scalar sector, we collect the mass matrix of the neutral gauge bosons. This term is given by

$$\mathcal{L}_K \supset \frac{1}{2}V_0^T M_G^2 V_0, \tag{14}$$

where

Table 1. Table of matter fields, scalar bosons with their charge quantum numbers of the vector $B-L$ model. We omit the index of generations of matter particles in this Table. In this paper, we note N_i as three RHNs for later uses.

Fields	$SU(3)_c \otimes SU(2)_L \otimes U(1)_Y \otimes U(1)_{B-L}$
L_L	$(1,2,-\frac{1}{2},-1)$
Q_L	$(3,2,\frac{1}{6},\frac{1}{3})$
e_R	$(1,1,-1,-1)$
ν_R	$(1,1,0,-1)$
u_R	$(3,1,\frac{2}{3},\frac{1}{3})$
d_R	$(3,1,-\frac{1}{3},\frac{1}{3})$
Φ	$(1,2,\frac{1}{2},0)$
χ	$(1,1,0,2)$

$V_0^T = \begin{pmatrix} B_\mu & W_{3\mu} & X_\mu \end{pmatrix}$ and

$$M_G^2 = \begin{pmatrix} \frac{1}{4}g'^2 v_\Phi^2 & -\frac{1}{4}gg' v_\Phi^2 & 0 \\ -\frac{1}{4}gg' v_\Phi^2 & \frac{1}{4}g^2 v_\Phi^2 & 0 \\ 0 & 0 & g_1'^2 v_\chi^2 \end{pmatrix}. \tag{15}$$

When we consider the mixing of two $U(1)_Y, U(1)_{B-L}$ gauges, one first uses the rotation matrix in Eq. (2) for obtaining the basis $(\tilde{B}_\mu\ \tilde{X}_\mu)$. To find the physical masses of gauge bosons, we have to diagonalize the mass matrix in the basis $\tilde{V}_0^T = (\tilde{B}_\mu\ W_{3\mu}\ \tilde{X}_\mu)$. First, the mass matrix of the neutral gauge bosons in the kinetic term diagonalized basis $\tilde{V}_0^T = (\tilde{B}_\mu\ W_{3\mu}\ \tilde{X}_\mu)$ can be collected as follows:

$$\mathcal{L}_K \supset \frac{1}{2}\tilde{V}_0^T S^T M_G^2 S\, \tilde{V}_0 = \frac{1}{2}\tilde{V}_0^T \tilde{M}_G^2 \tilde{V}_0, \tag{16}$$

where

$$S = \begin{pmatrix} 1 & 0 & -\frac{\kappa}{\sqrt{1-\kappa^2}} \\ 0 & 1 & 0 \\ 0 & 0 & \frac{1}{\sqrt{1-\kappa^2}} \end{pmatrix},$$

$$\tilde{M}_G^2 = S^T M_G^2 S = \begin{pmatrix} \frac{1}{4}g'^2 v_\Phi^2 & -\frac{1}{4}gg' v_\Phi^2 & \frac{1}{4}g'\tilde{g}_t v_\Phi^2 \\ -\frac{1}{4}gg' v_\Phi^2 & \frac{1}{4}g^2 v_\Phi^2 & -\frac{1}{4}g\tilde{g}_t v_\Phi^2 \\ \frac{1}{4}g'\tilde{g}_t v_\Phi^2 & -\frac{1}{4}g\tilde{g}_t v_\Phi^2 & \frac{1}{4}\tilde{g}_t^2 v_\Phi^2 + g_1''^2 v_\chi^2 \end{pmatrix} \tag{17}$$

with the new coupling $\tilde{g}_t = -\frac{g'\kappa}{\sqrt{1-\kappa^2}}$. By changing the basis from $\tilde{B}^\mu$, $W_3^\mu, \tilde{X}^\mu$ to the one in A^μ, Z^μ, Z'^μ, we have the mass eigenstates for physical gauge bosons. The relation is shown in the following rotation matrix as

$$\begin{pmatrix} \tilde{B}_\mu \\ W_3^\mu \\ \tilde{X}_\mu \end{pmatrix} = \begin{pmatrix} c_W & -s_W c_{BL} & s_W s_{BL} \\ s_W & c_W c_{BL} & -c_W s_{BL} \\ 0 & s_{BL} & c_{BL} \end{pmatrix} \begin{pmatrix} A_\mu \\ Z_\mu \\ Z'^\mu \end{pmatrix}. \tag{18}$$

Here, $s_W(c_W) = \sin\theta_W(\cos\theta_W)$ and $s_{BL}(c_{BL}) = \sin\theta_{BL}(\cos\theta_{BL})$ are mixing angles of gauge bosons. In the above formulas, we have the following parameters:

$$t_{2(BL)} = \frac{2\tilde{g}_t\sqrt{g^2+g'^2}}{\tilde{g}_t^2 + 16\left(\frac{v_\chi}{2v_\Phi}\right)^2 g_1''^2 - g^2 - g'^2} \text{ with}$$

$$g_1'' = \frac{g_1'}{\sqrt{1-\kappa^2}} = \frac{g_X q_X}{\sqrt{1-\kappa^2}}. \tag{19}$$

The masses of the physical gauge bosons A, Z, and Z' are expressed as

$$M_A = 0,\ M_{Z,Z'}^2 = \frac{1}{8}\left(Cv_\Phi^2 \mp \sqrt{-D + v_\Phi^4 C^2}\right), \tag{20}$$

where

$$C = g^2 + g'^2 + \tilde{g}_t^2 + 16\left(\frac{v_\chi}{2v_\Phi}\right)^2 g_1''^2,$$
$$D = 16 v_\Phi^2 v_\chi^2 (g^2 + g'^2) g_1''^2. \tag{21}$$

The covariant derivative with the kinetic mixing can be expressed in terms of the orthogonal fields $\tilde{B}$ and $\tilde{X}$ as

$$\begin{aligned} D_\mu &= \partial_\mu - \mathrm{i}g_s T^a G_\mu^a - \mathrm{i}g T^a W_\mu^a - \mathrm{i}g' Y \tilde{B}_\mu \\ &\quad - \mathrm{i}\left(g_X Y_X \frac{1}{\sqrt{1-\kappa^2}} - g' Y \frac{\kappa}{\sqrt{1-\kappa^2}}\right)\tilde{X}_\mu \\ &= \partial_\mu - \mathrm{i}g_s T^a G_\mu^a - \mathrm{i}g T^a W_\mu^a \\ &\quad - \mathrm{i}g' Y \tilde{B}_\mu - \mathrm{i}(\tilde{g}_X Y_X + \tilde{g}_t Y)\tilde{X}_\mu. \end{aligned} \tag{22}$$

Here, $\tilde{g}_X = g_X \frac{1}{\sqrt{1-\kappa^2}}$. In the case of the non-kinematic mixing gauge, taking $\kappa \to 0$, one has the covariant derivative as

$$D_\mu = \partial_\mu - \mathrm{i}g_s T^a G_\mu^a - \mathrm{i}g T^a W_\mu^a - \mathrm{i}g' Y B_\mu - \mathrm{i}g_X Y_X X_\mu. \tag{23}$$

The neutrino masses in this model are generated by a seesaw mechanism that will be shown in the Yukawa Lagrangian, namely,

$$\begin{aligned} -\mathcal{L}_Y &= \mathcal{L}_{SM} + Y_\nu \bar{L}\tilde{\Phi}\nu_R + \frac{Y_M}{2}\bar{\nu_R^c}\nu_R\chi + H.c \\ &\supset \frac{Y_\nu v_\Phi}{\sqrt{2}}\bar{\nu_L}\nu_R + \frac{Y_\nu c_\theta}{\sqrt{2}}\bar{\nu_L} h \nu_R + \frac{y_M v_\Phi}{2\sqrt{2}}\bar{\nu_R^c}\nu_R \\ &\quad - \frac{y_M s_\theta}{2\sqrt{2}}\bar{\nu_R^c} h \nu_R + H.c. \end{aligned} \tag{24}$$

where $\tilde{\Phi} = \mathrm{i}\sigma_2\Phi^*$, the Dirac mass is $m_D = \frac{Y_\nu v_\Phi}{\sqrt{2}}$, and the Majorana mass is $M_R = \frac{y_M v_\chi}{\sqrt{2}}$. The Yukawa Lagrangian shows that the χ field generates the Majorana mass and Φ

generates the Dirac masses for the RHNs.

The fermion Lagrangian is given by

$$\begin{aligned}\mathcal{L}_f &= \mathcal{L}_f^{SM} + \mathrm{i}\bar{\nu}_R\gamma_\mu D^\mu \nu_R \\ &= \mathrm{i}\bar{q}_L\gamma_\mu D^\mu q_L + \mathrm{i}\bar{u}_R\gamma_\mu D^\mu u_R + \mathrm{i}\bar{d}_R\gamma_\mu D^\mu d_R \\ &\quad + \mathrm{i}\bar{l}_L\gamma_\mu D^\mu l_L + \mathrm{i}\bar{e}_R\gamma_\mu D^\mu e_R + \mathrm{i}\bar{\nu}_R\gamma_\mu D^\mu \nu_R. \end{aligned} \tag{25}$$

All couplings involving the processes under consideration are presented in the following Tables 2, 3, 4, 5. In Table 2, the third column is presented for the couplings in the second column by changing the bare parameters to physical parameters accordingly. The last column presents the results of the corresponding couplings in the limit of non-kinematic mixing.

Table 3 presents the couplings of the SM-like Higgs to Z and Z' related to the computed processes. The last column lists the results of the corresponding couplings in the case of non-kinematic mixing.

In Table 4, three gauge boson vertices related to the processes are presented. The corresponding couplings in non-kinematic mixing are listed in the last column results.

In Table 5, all the couplings of Zff and $Z'ff$ are presented. Hypercharge Y_X^f takes the corresponding values for f presented in Table 1. Here, $P_{L,R} = \frac{1-\gamma_5}{2}$ and $\tilde{g}_X = g_X/\sqrt{1-\kappa^2}$. Again, the corresponding couplings in the case of non-kinematic mixing are presented in the last

Table 2. Couplings related to the processes under consideration. In some cases, we have used the following relations: $M_W = \frac{g v_\Phi}{2}$, $e = g s_W = g' c_W$ and $\tilde{g}_t = -g'\frac{\kappa}{\sqrt{1-\kappa^2}}$.

Vertices	Mixing	Mixing (physical parameters)	Non-mixing
hW^-W^+	$\frac{g^2 v_\Phi}{2} c_\theta g_{\mu\nu}$	$\frac{eM_W}{s_W} c_\theta g_{\mu\nu}$	–
hW^+G^-	$\frac{g}{2} c_\theta (p_\mu^h - p_\mu^{G^-})$	$\frac{e}{2s_W} c_\theta (p_\mu^h - p_\mu^{G^-})$	–
hW^-G^+	$\frac{g}{2} c_\theta (p_\mu^{G^+} - p_\mu^h)$	$\frac{e}{2s_W} c_\theta (p_\mu^{G^+} - p_\mu^h)$	–
$AW^\pm G^\mp$	$\frac{g g' c_W v_\Phi}{2} g_{\mu\nu}$	$eM_W g_{\mu\nu}$	–
AG^+G^-	$\frac{g s_W + g' c_W}{2}(p_\mu^+ - p_\mu^-)$	$e(p_\mu^+ - p_\mu^-)$	–
ZG^+G^-	$[\frac{g c_W - g' s_W}{2} c_{BL} + \frac{\tilde{g}_t}{2} s_{BL}](p_\mu^+ - p_\mu^-)$	$[\frac{e c_{2W}}{s_{2W}} c_{BL} + \frac{\tilde{g}_t}{2} s_{BL}](p_\mu^+ - p_\mu^-)$	$\frac{e\, c_{2W}}{s_{2W}}(p_\mu^+ - p_\mu^-)$
$Z'G^+G^-$	$[\frac{-g c_W + g' s_W}{2} s_{BL} + \frac{\tilde{g}_t}{2} c_{BL}](p_\mu^+ - p_\mu^-)$	$[\frac{-e c_{2W}}{s_{2W}} s_{BL} + \frac{\tilde{g}_t}{2} c_{BL}](p_\mu^+ - p_\mu^-)$	0
$ZW^\pm G^\mp$	$\frac{g v_\Phi}{2}[-g' s_W c_{BL} + \tilde{g}_t s_{BL}]\, g_{\mu\nu}$	$M_W[-e\frac{s_W}{c_W} c_{BL} + \tilde{g}_t s_{BL}]\, g_{\mu\nu}$	$-\frac{eM_W s_W}{c_W} g_{\mu\nu}$
$Z'W^\pm G^\mp$	$\frac{g v_\Phi}{2}[g' s_W s_{BL} + \tilde{g}_t c_{BL}]\, g_{\mu\nu}$	$M_W[e\frac{s_W}{c_W} s_{BL} + \tilde{g}_t c_{BL}]\, g_{\mu\nu}$	0
hG^+G^-	$\lambda_\Phi v_\Phi \left(c_\theta + \frac{v_\Phi}{v_\chi} s_\theta\right) + 2m_\Phi^2 \frac{s_\theta}{v_\chi}$	$\frac{M_h^2}{v_\Phi} c_\theta$	–

Table 3. Couplings of the SM-like Higgs to Z and Z' related to the processes under consideration. In some cases, we have used the following relations: $M_W = \frac{g v_\Phi}{2}, e = g s_W = g' c_W$. Here, $s_{2(BL)} = 2 s_{BL} c_{BL}$.

Vertices	Mixing	Non-mixing ($\kappa = 0, s_{BL} = 0$)
hZZ'	$[\tilde{g}_X^2 Y_X^2 v_\chi s_\theta s_{2(BL)} - \frac{1}{2}(\frac{e}{s_W c_W} c_{BL} - \tilde{g}_t s_{BL}) \times (\frac{e}{s_W c_W} s_{BL} + \tilde{g}_t c_{BL}) v_\Phi c_\theta] g_{\mu\nu}$	0
hZZ	$[2\tilde{g}_X^2 Y_X^2 v_\chi s_\theta\, s_{BL}^2 + \frac{v_\Phi c_\theta}{2}(\frac{e}{s_W c_W} c_{BL} - \tilde{g}_t s_{BL})^2] g_{\mu\nu}$	$\left(\frac{eM_W}{c_W^2 s_W} c_\theta\right) g_{\mu\nu}$
$hZ'Z'$	$[2\tilde{g}_X^2 Y_X^2 v_\chi s_\theta\, c_{BL}^2 + \frac{v_\Phi c_\theta}{2}(\frac{e}{s_W c_W} s_{BL} + \tilde{g}_t c_{BL})^2] g_{\mu\nu}$	$\left(2 g_X^2 Y_X^2 v_\chi s_\theta\right) g_{\mu\nu}$

Table 4. Couplings of three gauge boson vertices related to the processes under consideration.

Vertices	Mixing	Non-mixing
$A_\rho W_\nu^- W_\mu^+$	$e[(p_1-p_3)^\nu g^{\rho\mu} - (p_1-p_2)^\rho g^{\mu\nu} - (p_2-p_3)^\mu g^{\rho\nu}]$	–
$Z_\rho W_\nu^- W_\mu^+$	$e\frac{c_W}{s_W} c_{BL}[(p_1-p_3)^\nu g^{\rho\mu} - (p_1-p_2)^\rho g^{\mu\nu} - (p_2-p_3)^\mu g^{\rho\nu}]$	$-\vert_{c_{BL}\to 1}$
$Z'_\rho W_\nu^- W_\mu^+$	$-e\frac{c_W}{s_W} s_{BL}[(p_1-p_3)^\nu g^{\rho\mu} - (p_1-p_2)^\rho g^{\mu\nu} - (p_2-p_3)^\mu g^{\rho\nu}]$	0

Table 5. Couplings related to the processes under consideration. In some cases, we have used the following relations: $M_W = \frac{g v_\Phi}{2}$, $e = g s_W = g' c_W$. Hypercharge Y_X^f takes the corresponding values for f presented in Table 1. Here, $P_{L,R} = \frac{1-\gamma_5}{2}$ and $\tilde{g}_X = \frac{g_X}{\sqrt{1-\kappa^2}}$.

Vertices	Mixing	Non-mixing
$Z_\mu \bar{f} f$	$-\frac{e}{s_W c_W}\gamma_\mu[(I_3^f - s_W^2 Q_f)P_L - s_W^2 Q_f P_R]c_{BL}$	
	$-\gamma_\mu[(\tilde{g}_X Y_X^f + \tilde{g}_t Y_{f_L})P_L + (\tilde{g}_X Y_X^f + \tilde{g}_t Y_{f_R})P_R]s_{BL}$	$-\vert_{\kappa\to 0, c_{BL}\to 1}$
$Z'_\mu \bar{f} f$	$\frac{e}{s_W c_W}\gamma_\mu[(I_3^f - s_W^2 Q_f)P_L - s_W^2 Q_f P_R]s_{BL}$	
	$-\gamma_\mu[(\tilde{g}_X Y_X^f + \tilde{g}_t Y_{f_L})P_L + (\tilde{g}_X Y_X^f + \tilde{g}_t Y_{f_R})P_R]c_{BL}$	$-g_X\, Y_X^f \gamma_\mu$

column results.

B. Chiral $B-L$ model

In this section, we discuss another version of the $U(1)_{B-L}$ extension of the SM, which is the chiral $B-L$ model. In this version of the $B-L$ model, together with three right-handed neutrinos, we have an extra doublet φ and an scalar singlet σ. The matter field contents, scalar fields, and their quantum numbers are presented in Table 6. The generation indices for matter particles are suppressed.

This model also adds an additional scalar Dark matter χ_d, which plays a role of dark matter. In general, the scalar sector takes the form of

$$\begin{aligned}\mathcal{L}_H &= \mathcal{L}_K - \mathcal{V}(\Phi,\varphi,\sigma,\chi_d)\\ &= (D_\mu\Phi)^\dagger D_\mu\Phi + (D_\mu\varphi)^\dagger D_\mu\varphi + (D_\mu\sigma)^\dagger D_\mu\sigma\\ &\quad + (D_\mu\chi_d)^\dagger D_\mu\chi_d - \mathcal{V}(\Phi,\varphi,\sigma,\chi_d).\end{aligned} \tag{26}$$

Here, the covariant derivative is defined in (23). The scalar potential is expressed as follows:

$$\begin{aligned}\mathcal{V}(\Phi,\varphi,\sigma,\chi_d) &= m_\sigma^2(\sigma^*\sigma) + \frac{1}{2}\lambda_\sigma(\sigma^*\sigma)^2 + m_\Phi^2\left(\Phi^\dagger\Phi\right)\\ &+ \frac{1}{2}\lambda_\Phi\left(\Phi^\dagger\Phi\right)^2 + m_\varphi^2\left(\varphi^\dagger\varphi\right) + \frac{1}{2}\lambda_\varphi\left(\varphi^\dagger\varphi\right)^2\\ &+ m_{\chi_d}^2\left(\chi_d^*\chi_d\right) + \frac{1}{2}\lambda_{\chi_d}\left(\chi_d^*\chi_d\right)^2 - \mu\left(\Phi^\dagger\varphi\right)\sigma\\ &- \mu\left(\varphi^\dagger\Phi\right)\sigma^* + \lambda_{\Phi\sigma}\left(\Phi^\dagger\Phi\right)(\sigma\sigma^*)\\ &+ \lambda_{\varphi\sigma}\left(\varphi^\dagger\varphi\right)(\sigma\sigma^*) + \lambda_{\Phi\varphi_1}\left(\Phi^\dagger\Phi\right)\left(\varphi^\dagger\varphi\right)\\ &+ \lambda_{\Phi\varphi_2}\left(\Phi^\dagger\varphi\right)\left(\varphi^\dagger\Phi\right) + \lambda_{\Phi\chi_d}\left(\Phi^\dagger\Phi\right)\left(\chi_d^*\chi_d\right)\\ &+ \lambda_{\varphi\chi_d}\left(\varphi^\dagger\varphi\right)\left(\chi_d^*\chi_d\right) + \lambda_{\sigma\chi_d}(\sigma^*\sigma)\left(\chi_d^*\chi_d\right).\end{aligned} \tag{27}$$

The fields Φ, φ, and σ can be written for the SSB as follows:

$$\Phi = \frac{1}{\sqrt{2}}\begin{pmatrix}\sqrt{2}G_1^\pm\\ v_\Phi + R_1 + \mathrm{i}I_1\end{pmatrix},$$

Table 6. Matter fields and their quantum numbers of the chiral $B-L$ model. We omit the index of generations of matter particles in this Table. In this work, we note right handed neutrinos as N_i for $i = 1,2,3$ for latter uses.

Fields	$SU(3)_C \otimes SU(2)_L \otimes U(1)_Y \otimes U(1)_{B-L}$
L_L	$(1,2,-1/2,-1)$
Q_L	$(3,2,1/6,1/3)$
e_R	$(1,1,-1,-1)$
u_R	$(3,1,2/3,1/3)$
d_R	$(3,1,-1/3,1/3)$
ν_R^1	$(1,1,0,5)$
$\nu_R^{2,3}$	$(1,1,0,-4)$
Φ	$(1,2,1/2,0)$
φ	$(1,2,1/2,-3)$
σ	$(1,1,0,3)$
χ_d	$(1,1,0,1/2)$

$$\varphi = \frac{1}{\sqrt{2}}\begin{pmatrix}\sqrt{2}G_2^\pm\\ v_\varphi + R_2 + \mathrm{i}I_2\end{pmatrix}, \quad \sigma = \frac{1}{\sqrt{2}}(v_\sigma + R_3 + \mathrm{i}I_3) \tag{28}$$

In this role, the fields Φ and φ break the electroweak symmetry, whereas the scalar fields σ and φ break the $U(1)_{B-L}$ symmetry. The minimization for the scalar potential leads to the following system of equations:

$$2m_\Phi^2 + \lambda_\Phi v_\Phi^2 + \lambda_{\Phi\sigma}v_\sigma^2 + (\lambda_{\Phi\varphi_1} + \lambda_{\Phi\varphi_2})v_\varphi^2 - \frac{\sqrt{2}\mu v_\varphi v_\sigma}{v_\Phi} = 0, \tag{29}$$

$$2m_\sigma^2 + \lambda_\sigma v_\sigma^2 + \lambda_{\Phi\sigma}v_\Phi^2 + \lambda_{\varphi\sigma}v_\varphi^2 - \frac{\sqrt{2}\mu v_\Phi v_\varphi}{v_\sigma} = 0, \tag{30}$$

$$2m_\varphi^2 + \lambda_\varphi v_\varphi^2 + \lambda_{\varphi\sigma}v_\sigma^2 + (\lambda_{\Phi\varphi_1} + \lambda_{\Phi\varphi_2})v_\Phi^2 - \frac{\sqrt{2}\mu v_\Phi v_\sigma}{v_\varphi} = 0. \tag{31}$$

The mass matrix for charged Higgs is then collected in

term of the basics $(G_1^\pm, G_2^\pm)$ as

$$\mathcal{M}_\pm^2 = \frac{1}{2}\begin{pmatrix} \frac{\sqrt{2}\mu v_\sigma v_\varphi}{v_\Phi} - v_\varphi^2\lambda_{\Phi\varphi_2} & v_\Phi v_\varphi \lambda_{\Phi\varphi_2} - \sqrt{2}\mu v_\sigma \\ v_\Phi v_\varphi \lambda_{\Phi\varphi_2} - \sqrt{2}\mu v_\sigma & \frac{\sqrt{2}\mu v_\sigma v_\Phi}{v_\varphi} - v_\Phi^2\lambda_{\Phi\varphi_2} \end{pmatrix} \tag{32}$$

After symmetry breaking, this model contains Goldstone bosons $G^\pm$ and charged Higgs $H^\pm$, which are mixed by $G_1^\pm, G_2^\pm$. The Goldstone bosons $G^\pm$ give the masses to the $W^\pm$ bosons. The mixing matrix is given by

$$\begin{pmatrix} G^\pm \\ H^\pm \end{pmatrix} = \begin{pmatrix} c_\alpha & s_\alpha \\ -s_\alpha & c_\alpha \end{pmatrix}\begin{pmatrix} G_1^\pm \\ G_2^\pm \end{pmatrix}. \tag{33}$$

The mass matrix in the basis (I_1, I_2, I_3) can be written as

$$\mathcal{M}_I^2 = \frac{1}{\sqrt{2}}\begin{pmatrix} \frac{\mu v_\varphi v_\sigma}{v_\Phi} & -\mu v_\sigma & -\mu v_\varphi \\ -\mu v_\sigma & \frac{\mu v_\Phi v_\sigma}{v_\varphi} & \mu v_\Phi \\ -\mu v_\varphi & \mu v_\Phi & \frac{\mu v_\Phi v_\varphi}{v_\sigma} \end{pmatrix} \tag{34}$$

For the neutral components of Higgs fields, we have the following relation:

$$\begin{pmatrix} G_1^0 \\ G_2^0 \\ A_0 \end{pmatrix} = \begin{pmatrix} c_\alpha & s_\alpha & 0 \\ -s_\alpha c_\beta & c_\alpha c_\beta & -s_\beta \\ -s_\alpha s_\beta & c_\alpha s_\beta & c_\beta \end{pmatrix}\begin{pmatrix} I_1 \\ I_2 \\ I_3 \end{pmatrix},$$

with

$$t_\alpha = \frac{v_\varphi}{v_\Phi}, \quad t_\beta = \frac{v_\sigma v}{v_\Phi v_\varphi}. \tag{35}$$

After the EWSB, G_1^0, G_2^0 give the masses for Z and Z', respectively. The remaining physical field A_0 becomes a CP-odd Higgs boson. The masses of the charged and CP-odd Higgses are determined as follows:

$$M_{H^\pm}^2 = \frac{v^2}{2v_\Phi v_\varphi}(\sqrt{2}\mu v_\sigma - v_\Phi v_\varphi \lambda_{\Phi\varphi_2}), \tag{36}$$

$$M_{A_0}^2 = \frac{\mu}{\sqrt{2}v_\Phi v_\varphi v_\sigma}(v_\Phi^2 v_\varphi^2 + v_\sigma^2 v^2). \tag{37}$$

The mass matrix for neutral scalars is collected in the basis (R_1, R_2, R_3). It can be expressed in the form of

$$\mathcal{M}_S^2 = \frac{1}{2}\begin{pmatrix} 2v_\Phi^2\lambda_\Phi + \frac{\sqrt{2}\mu}{v_\Phi}v_\varphi v_\sigma & 2v_\Phi v_\varphi \lambda_{12} - \sqrt{2}\mu v_\sigma & 2v_\Phi v_\sigma \lambda_{\Phi\sigma} - \sqrt{2}v_\varphi \mu \\ 2v_\Phi v_\varphi \lambda_{12} - \sqrt{2}\mu v_\sigma & 2v_\varphi^2\lambda_\varphi + \frac{\sqrt{2}\mu}{v_\varphi}v_\Phi v_\sigma & 2v_\varphi v_\sigma \lambda_{\varphi\sigma} - \sqrt{2}v_\Phi \mu \\ 2v_\Phi v_\sigma \lambda_{\Phi\sigma} - \sqrt{2}v_\varphi \mu & 2v_\varphi v_\sigma \lambda_{\varphi\sigma} - \sqrt{2}v_\Phi \mu & 2v_\sigma^2\lambda_\sigma + \frac{\sqrt{2}\mu}{v_\sigma}v_\Phi v_\varphi, \end{pmatrix} \tag{38}$$

where $\lambda_{12} = \lambda_{\Phi\varphi_1} + \lambda_{\Phi\varphi_2}$. The matrix $\mathcal{M}_S^2$ can be diagonalized by an orthogonal matrix as

$$O_S^T M_S^2 O_S = \mathrm{diag}(M_{H_1}^2, M_{H_2}^2, M_{H_3}^2). \tag{39}$$

Here, the relation between the two basics is given by

$$\begin{pmatrix} H_1 \\ H_2 \\ H_3 \end{pmatrix} = O_S \begin{pmatrix} R_1 \\ R_2 \\ R_3 \end{pmatrix} \tag{40}$$

For CP-even scalar Higgses, the mass eigenstates are ordered by their masses $M_{H_1} \le M_{H_2} \le M_{H_3}$. In this notation, $h = H_1$ is identified as the SM Higgs of 125 GeV. The rotation matrix is defined as $O_S = \mathcal{R}_{23}\mathcal{R}_{13}\mathcal{R}_{12}$, where each matrix is expressed as follows:

$$\mathcal{R}_{12} = \begin{pmatrix} c_{12} & -s_{12} & 0 \\ s_{12} & c_{12} & 0 \\ 0 & 0 & 1 \end{pmatrix}, \mathcal{R}_{13} = \begin{pmatrix} c_{13} & 0 & -s_{13} \\ 0 & 1 & 0 \\ s_{13} & 0 & c_{13} \end{pmatrix},$$

$$\mathcal{R}_{23} = \begin{pmatrix} 1 & 0 & 0 \\ 0 & c_{23} & -s_{23} \\ 0 & s_{23} & c_{23} \end{pmatrix} \tag{41}$$

where $c_{ij} = \cos\theta_{ij}, s_{ij} = \sin\theta_{ij}$ with $-\frac{\pi}{2} \le \theta_{ij} \le \frac{\pi}{2}$.

The rotation matrix for neutral gauge bosons is

$$\begin{pmatrix} A^\mu \\ Z^\mu \\ Z'^\mu \end{pmatrix} = \begin{pmatrix} c_W & s_W & 0 \\ -c'_{BL}s_W & c'_{BL}c_W & -s'_{BL} \\ -s'_{BL}s_W & s'_{BL}c_W & c'_{BL} \end{pmatrix} \begin{pmatrix} B^\mu \\ W_3^\mu \\ X^\mu \end{pmatrix}, \tag{42}$$

and the masses of photon A, Z, Z' bosons are obtained as follows:

$$M_A = 0, \qquad M_Z^2 = \frac{v^2}{8}(A' - \sqrt{B'^2 + C'^2}),$$
$$M_{Z'}^2 = \frac{v^2}{8}(A' + \sqrt{B'^2 + C'^2}). \tag{43}$$

Here,

$$A' = 36\frac{v_\varphi^2 + v_\sigma^2}{v^2}g_X^2 + (g^2 + g'^2), \quad B' = 36\frac{v_\varphi^2 + v_\sigma^2}{v^2}g_X^2 - (g^2 + g'^2), \tag{44}$$

It is noted that we have not considered the kinematic mixing of the two gauges $U(1)_Y$ and $U(1)_{B-L}$. However, in this report, we assume the mixing case of two neutral gauge bosons Z, Z'.

The Yukawa Lagrangian of the model can be written as

$$-\mathcal{L}_Y = Y_e\bar{L}\Phi e_R + Y_u\bar{Q}\tilde{\Phi}u_R + Y_e\bar{Q}\Phi d_R + Y_\nu\bar{L}\tilde{\varphi}\nu_R + H.c$$
$$\supset \frac{Y_\nu v_\varphi}{\sqrt{2}}\bar{\nu_L}\nu_R + H.c \tag{45}$$

where the φ field generates a Dirac neutrino mass for the RHNs. This model does not have a Majorana mass term for ν_R.

Finally, the mass of dark matter from the Higgs potential is given as

$$M_{DM}^2 = \frac{2m_{\chi_d}^2 + v_\Phi^2\lambda_{\chi_d} + v_\sigma^2\lambda_{\sigma\chi_d} + v_\varphi^2\lambda_{\varphi\chi_d}}{2}. \tag{46}$$

In this version, we have two CP-even Higges, one CP-odd Higgs, and two charged Higgses. Furthermore, we have three more right handed neutrinos and a neutral gauge boson Z'. All these new particles are exchanged in the loop Feynman diagrams of the processes under consideration.

All couplings relating to the the computed processes are presented in the following Tables 7, 8, 9, 10, and 11. In several cases, we have used $M_W = \frac{1}{2}g\sqrt{v_\Phi^2 + v_\varphi^2}$, $s_\alpha = \frac{v_\varphi}{v}$, $c_\alpha = \frac{v_\Phi}{v}$, $e = gs_W = g'c_W$. In Table 7, the third column results correspond to the couplings in the second column by replacing the bare parameters in the Lagrangian with the physical parameters. The last column shows for the results of the non-mixing two gauge bosons.

The couplings of $hH^\pm H^\mp$ and $hG^\pm G^\mp$ are given by

$$\begin{aligned} g_{hH^\pm H^\mp} = {} & \lambda_\Phi v_\Phi c_{13}c_{12}s_\alpha^2 - \lambda_\varphi v_\varphi c_{13}s_{12}c_\alpha^2 \\ & - \frac{\mu}{\sqrt{2}}s_{13}s_\alpha c_\alpha - \frac{\mu}{\sqrt{2}}s_{13}s_\alpha c_\alpha \\ & - \lambda_{\Phi\sigma}v_\sigma s_\alpha^2 s_{13} - \lambda_{\varphi\sigma}v_\sigma c_\alpha^2 s_{13} \\ & + \lambda_{\Phi\varphi_1}[-c_{13}s_{12}s_\alpha^2 v_\varphi + c_{13}c_{12}c_\alpha^2 v_\Phi] \\ & - \lambda_{\Phi\varphi_2}(-v_\Phi c_{13}s_{12} + v_\varphi c_{13}c_{12})s_\alpha c_\alpha, \end{aligned} \tag{47}$$

Table 7. Couplings related to the processes under consideration. In some cases, we have used $M_W = \frac{1}{2}g\sqrt{v_\Phi^2 + v_\varphi^2}$, $s_\alpha = \frac{v_\varphi}{v}$, $c_\alpha = \frac{v_\Phi}{v}$, $e = gs_W = g'c_W$. The vector $B-L$ can be obtained by taking the limits of $c_{12} \to 1, c_{23} \to 1$ and $s'_{BL} \to -s_{BL}$.

Vertices	Mixing	Mixing (physical parameters)	Non-mixing
$hW^\pm W^\mp$	$\frac{g^2}{2}(v_\Phi c_{13}c_{12} - v_\varphi c_{13}s_{12})\, g_{\mu\nu}$	$\frac{eM_W}{s_W}c_{\alpha+\widehat{12}}c_{13}$	–
$Z'W^\pm G^\mp$	$-\frac{gg's_W(c_\alpha v_\Phi + s_\alpha v_\varphi)}{2}s'_{BL}$	$-\frac{eM_W s_W}{c_W}s'_{BL}$	0
$ZW^\pm G^\mp$	$-\frac{gg's_W(c_\alpha v_\Phi + s_\alpha v_\varphi)c'_{BL}}{2}$	$-\frac{eM_W s_W}{c_W}c'_{BL}$	$-\vert_{c'_{BL}=1}$
hW^+G^-	$\frac{gc_{13}(c_{12}c_\alpha - s_{12}s_\alpha)}{2}(p_\mu^h - p_\mu^{G^-})$	$\frac{e}{2s_W}c_{\alpha+\widehat{12}}c_{13}(p_\mu^h - p_\mu^{G^-})$	–
hW^-G^+	$-\frac{gc_{13}(c_{12}c_\alpha - s_{12}s_\alpha)}{2}(p_\mu^h - p_\mu^{G^+})$	$-\frac{e}{2s_W}c_{\alpha+\widehat{12}}c_{13}(p_\mu^h - p_\mu^{G^+})$	–
$AG^\pm G^\mp$	$\frac{(gs_W + g'c_W)}{2}(p_\mu^+ - p_\mu^-)^G$	$e(p_\mu^+ - p_\mu^-)^G$	–
$ZG^\pm G^\mp$	$\frac{(gc_W - g's_W)c'_{BL}}{2}(p_\mu^+ - p_\mu^-)^G$	$e\frac{c_{2W}}{s_{2W}}c'_{BL}(p_\mu^+ - p_\mu^-)^G$	$-\vert_{c'_{BL}=1}$
$Z'G^\pm G^\mp$	$\frac{(gc_W - g's_W)s'_{BL}}{2}(p_\mu^+ - p_\mu^-)^G$	$e\frac{c_{2W}}{s_{2W}}s'_{BL}(p_\mu^+ - p_\mu^-)^G$	0
$AH^\pm H^\mp$	$\frac{(gs_W + g'c_W)}{2}(p_\mu^+ - p_\mu^-)^H$	$e(p_\mu^+ - p_\mu^-)^H$	–
$ZH^\pm H^\mp$	$\frac{(gc_W - g's_W)c'_{BL}}{2}(p_\mu^+ - p_\mu^-)^H$	$e\frac{c_{2W}}{s_{2W}}c'_{BL}(p_\mu^+ - p_\mu^-)^H$	–
$Z'H^\pm H^\mp$	$\frac{(gc_W - g's_W)s'_{BL}}{2}(p_\mu^+ - p_\mu^-)^H$	$e\frac{c_{2W}}{s_{2W}}s'_{BL}(p_\mu^+ - p_\mu^-)^H$	0

Table 8. Couplings $hZZ, hZ'Z'$ in the chiral $B-L$ model. We have already taken into account $Y_X^2 = Y_X^2(\sigma) = Y_X^2(\varphi) = (\pm 3)^2$. The vector $B-L$ can be obtained by taking the limits of $c_{12} \to 1, c_{23} \to 1$ and $s'_{BL} \to -s_{BL}$.

Vertices	Mixing	Non-mixing
hZZ	$[2\, g_X^2 Y_X^2 (v_\sigma s_{13} - v_\varphi c_{13} s_{12}) s'^2_{BL} + \frac{eM_W}{s_W c_W^2} c_{\alpha+\widehat{12}} c_{13} c'^2_{BL}] g_{\mu\nu}$	$-\vert_{c'_{BL}=1}$
$hZ'Z'$	$[2 g_X^2 Y_X^2 (v_\sigma s_{13} - v_\varphi c_{13} s_{12}) c'^2_{BL} + \frac{eM_W}{s_W c_W^2} c_{\alpha+\widehat{12}} c_{13} s'^2_{BL}] g_{\mu\nu}$	$-\vert_{c'_{BL}=1}$
hZZ'	$[\frac{eM_W}{2 s_W c_W^2} c_{\alpha+\widehat{12}} c_{13} + g_X^2 Y_X^2 (v_\varphi c_{13} s_{12} - v_\sigma s_{13})] s_{2(BL)'}\, g_{\mu\nu}$	0

Table 9. Couplings of three gauge bosons in the chiral $B-L$ model, which are related to the processes under consideration. The vector $B-L$ model can be derived by applying $s'_{BL} \to -s_{BL}$.

Vertices	Mixing	Non-mixing
$A_\rho W_\nu^- W_\mu^+$	$e\,[(p_1-p_3)^\nu g^{\rho\mu} - (p_1-p_2)^\rho g^{\mu\nu} - (p_2-p_3)^\mu g^{\rho\nu}]$	–
$Z_\rho W_\nu^- W_\mu^+$	$\frac{ec_W}{s_W} c'_{BL}\, [(p_1-p_3)^\nu g^{\rho\mu} - (p_1-p_2)^\rho g^{\mu\nu} - (p_2-p_3)^\mu g^{\rho\nu}]$	$-\vert_{c'_{BL}=1}$
$Z'_\rho W_\nu^- W_\mu^+$	$\frac{ec_W}{s_W} s'_{BL} [(p_1-p_3)^\nu g^{\rho\mu} - (p_1-p_2)^\rho g^{\mu\nu} - (p_2-p_3)^\mu g^{\rho\nu}]$	0

Table 10. Couplings of the Z and Z' bosons to the fermion pair in the chiral $B-L$ model, which are related to the processes under consideration. The vector $B-L$ model can be derived by applying $s'_{BL} \to -s_{BL}$. Hypercharge Y_X^f takes the corresponding values for f presented in Table 1. Here, $P_{L,R} = \frac{1-\gamma_5}{2}$ and $\tilde{g}_X = \frac{g_X}{\sqrt{1-\kappa^2}}$.

Vertices	Mixing	Non-mixing
$Z_\mu \bar{f} f$	$-\frac{e}{s_W c_W} \gamma_\mu [(I_3^f - s_W^2 Q_f) P_L - s_W^2 Q_f P_R] c'_{BL} + \gamma_\mu (g_X Y_X^f) s'_{BL}$	$-\vert_{c'_{BL}\to 1}$
$Z'_\mu \bar{f} f$	$-\frac{e}{s_W c_W} \gamma_\mu [(I_3^f - s_W^2 Q_f) P_L - s_W^2 Q_f P_R] s'_{BL} - \gamma_\mu (g_X Y_X^f) c'_{BL}$	$-g_X Y_X^f \gamma_\mu$

$$
\begin{aligned}
g_{hG^\pm G^\mp} = {} & \lambda_\Phi v_\Phi c_{13} c_{12} c_\alpha^2 - \lambda_\varphi v_\varphi c_{13} s_{12} s_\alpha^2 \\
& + \frac{\mu}{\sqrt{2}} s_{13} s_\alpha c_\alpha + \frac{\mu}{\sqrt{2}} s_{13} s_\alpha c_\alpha \\
& - \lambda_{\Phi\sigma} v_\sigma c_\alpha^2 s_{13} - \lambda_{\varphi\sigma} v_\sigma s_\alpha^2 s_{13} \\
& + \lambda_{\Phi\varphi_1} [-c_{13} s_{12} c_\alpha^2 v_\varphi + c_{13} c_{12} s_\alpha^2 v_\Phi] \\
& + \lambda_{\Phi\varphi_2} (-v_\Phi c_{13} s_{12} + v_\varphi c_{13} c_{12}) s_\alpha c_\alpha. \qquad (48)
\end{aligned}
$$

We stress that the corresponding couplings in the vector $B-L$ can be derived by taking the limits of $c_{12} \to 1, c_{23} \to 1$, $c_{13} \to c_\theta$, $v_\Phi \to v$, and $s'_{BL} \to -s_{BL}$. In these limits, for example, the results of the third column in Table 7 are returned to the third column couplings in Table 2.

III. ONE-LOOP FORM FACTORS FOR $h \to \ell\bar{\ell}\gamma$ AND $e^-e^+ \to h\gamma$ IN THE $U(1)_{B-L}$ MODELS

One-loop form factors for $h \to \ell\bar{\ell}\gamma$ and $e^-e^+ \to h\gamma$ in the $U(1)_{B-L}$ models are presented in detail in this section. First, we presents the calculations for one-loop form factors for $h \to \ell\bar{\ell}\gamma$. We then show that the cross-sections for $e^-e^+ \to h\gamma$ can be derived by using one-loop form factors in the decay process $h \to \ell\bar{\ell}\gamma$.

Table 11. Couplings of neutral gauge bosons to Ghost particles in the chiral $B-L$ model, which are related to the processes under consideration. The vector $B-L$ model can be derived by applying $s'_{BL} \to -s_{BL}$. A denotes the photon field and p represents the four momenta of u^+.

Vertices	Mixing	Non-mixing
$A\bar{u}^\pm u^\mp$	$\mp i e\, p^\mu$	–
$Z'\bar{u}^\pm u^\mp$	$\mp i \frac{e}{s_W} c_W s'_{BL}\, p^\mu$	0
$Z\bar{u}^\pm u^\mp$	$\mp i \frac{e}{s_W} c_W c'_{BL}\, p^\mu$	$\mp i \frac{e}{s_W} c_W\, p^\mu$

A. Form factors for the decay process $h \to \ell\bar{\ell}\gamma$

In this section, we present the calculations for one-loop form factors for the decay channels $h \to \ell\bar{\ell}\gamma$ in the $U(1)_{B-L}$ extension of the SM. In this computation, all the new couplings that appear in the $U(1)_{B-L}$ models are denoted as g_{Vertices}. For the cases of the couplings of the SM-like Higgs to the vector boson pair and fermion pair, we parameterize as

$$
g_{hVV} = \kappa_{hVV} \cdot g_{hVV}^{\text{SM}}, \quad g_{hff} = \kappa_{hff} \cdot g_{hff}^{\text{SM}}. \qquad (49)
$$

All the couplings from the $B-L$ models involving the

processes are listed in the Tables in Sec. II. The factored couplings κ_{hff} and κ_{hVV} can be easily obtained from the above Tables.

Within the HF gauge, all one-loop Feynman diagrams contributing to the decay process are presented in the following paragraphs. These one-loop diagrams can be classified into several groups. In group 1 (a) (as shown in Fig. 1), we include all one-loop Feynman diagrams having V_0^*-poles contributing to the decay process. This means that we have $V_0^* \to \ell\bar{\ell}$ involved in these diagrams. In the current work, V_0^* can be γ^*, Z^*, and Z'^*. In the groups 1 (b), 1 (c) (as presented in Figs. 2, 3), other one-loop Feynman diagrams with V_0^*-poles are also plotted. In the HF gauge, we also take into account all fermions, charged Higgs, vector bosons, Goldstone bosons, and ghost particles propagating in the loop. As proved in Ref. [30], we only collect one-loop form factors, which are proportional to the $q_i^\mu q_3^\nu$ (for $i=1,2$) appearing in Eq. (50). Hence, all the diagrams in Fig. 2 and Fig. 3 can be ignored in the present work.

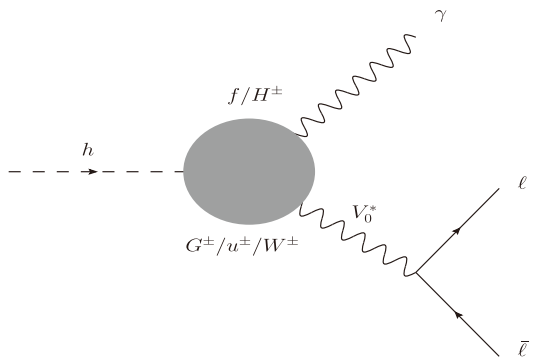

Fig. 1. Group 1(a)−One-loop Feynman diagram V_0^*-poles contributing to the processes. All the fermions, W bosons, charged Higgs, Goldstone bosons, and ghost particles exchanging in the loop are considered. V_0^* can be γ^*, Z^*, and Z'^* in this calculation.

In addition, three types of one-loop Feynman diagrams without V_0-poles (called non V_0-pole diagrams hereafter) contribute to the processes under consideration. The first classification includes non-V_0-pole diagrams with two neutral gauge bosons V_1, V_2 exchanging in the loop. In the calculation, V_1, V_2 can be Z^* and Z'^* in the loop (as depicted in Fig. 4). The second group includes non-V_0-pole with W bosons propagating in the loop (as presented in Fig. 5). The last category includes non-V_0-pole diagrams with charged Higgs propagating in the loop (as plotted in Fig. 6).

In general, the one-loop amplitude for the decay process of SM-like Higgs $h(p) \to \ell(q_1)\bar{\ell}(q_2)\gamma_\mu(q_3)$ can be expressed in terms of the Lorentz structure as follows:

$$\mathcal{A}^{h\to\ell\bar{\ell}\gamma}_{1-\text{loop}} = \sum_{i=\{1,2\}}\sum_{P=\{L,R\}} \Big\{\bar{v}(q_2)\Big(\gamma_\nu O_P\Big)\Big[F^P_{i,L}(q_i^\mu q_3^\nu) - F^P_{i,T}(q_i\cdot q_3)g^{\mu\nu}\Big]u(q_1)\Big\}\varepsilon^*_\mu(q_3) \tag{50}$$

where $O_{P=L,R} = \dfrac{1\mp\gamma_5}{2}$. Owing to the on-shell photon at

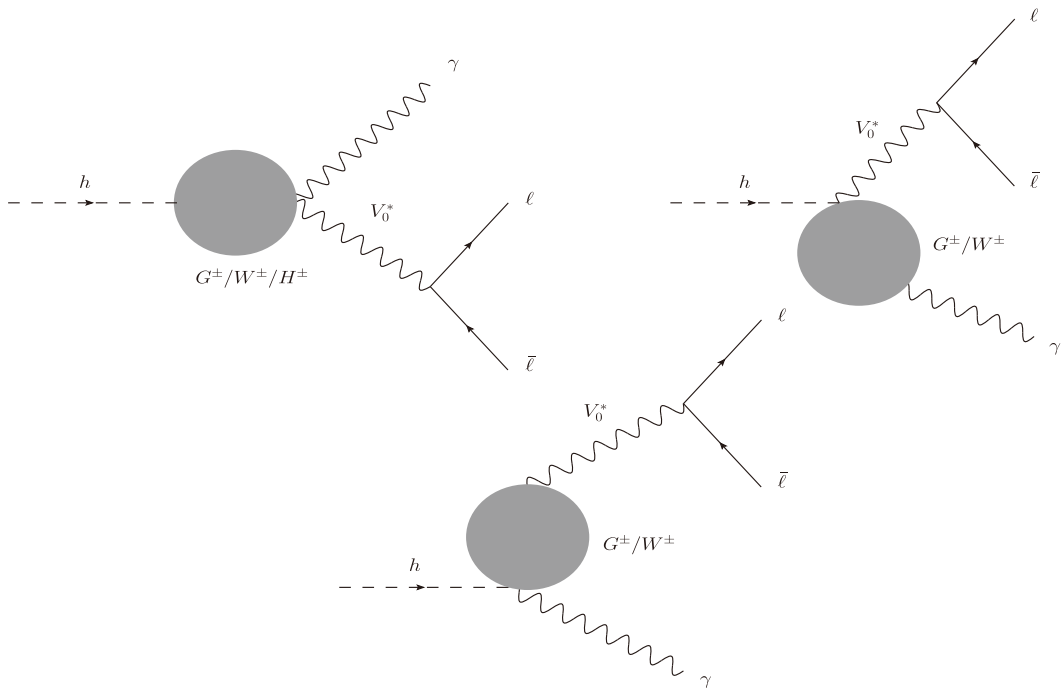

Fig. 2. Group 1(b)−One-loop Feynman diagram V_0^*-poles contributing to the processes. All the fermions, W bosons, charged Higgs, Goldstone bosons, and ghost particles exchanging in the loop are considered. V_0^* can be γ^*, Z^*, and Z'^* in this calculation.

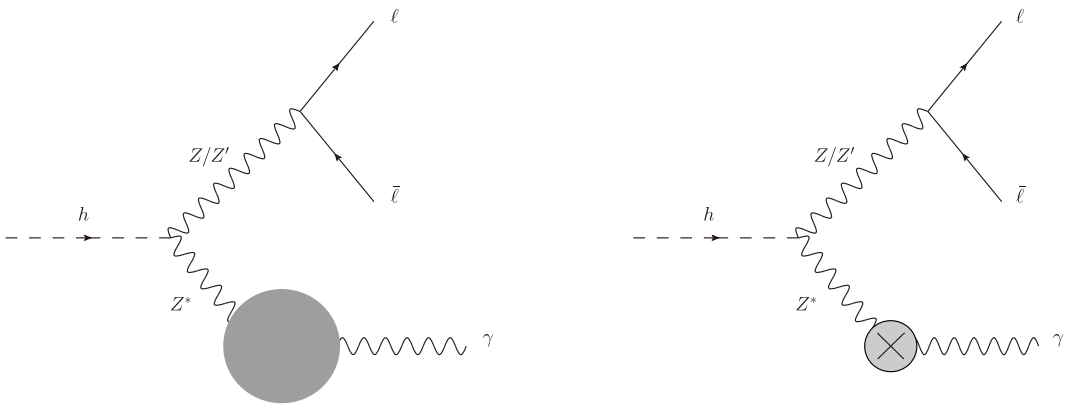

Fig. 3. Group $1(c)$–One-loop Feynman diagram V_0^*-poles contributing to the processes. All the fermions, W bosons, charged Higgs, Goldstone bosons, and ghost particles exchanging in the loop are considered. V_0^* can be γ^*, Z^*, and Z'^* in this calculation.

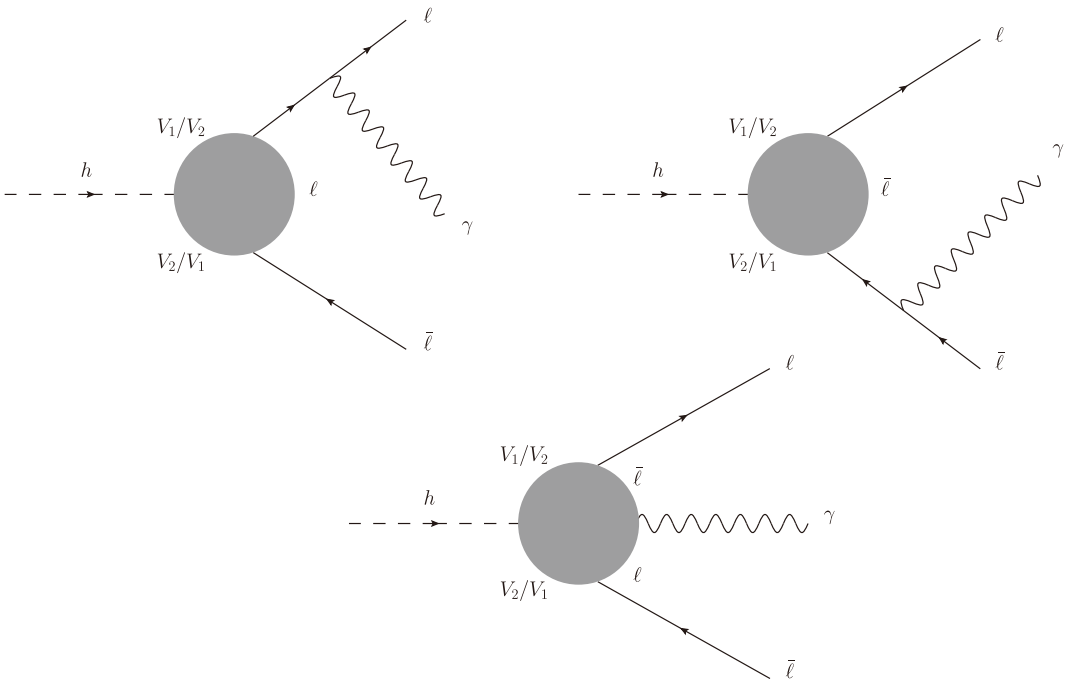

Fig. 4. One-loop Feynman non-V_0-pole diagrams with two neutral gauge bosons V_1, V_2 exchanging in the loop. In the calculation, V_1, V_2 can be Z^* and Z'^* in the loop.

the final state, the amplitude needs to follow ward identiy, and we can derive the relation $F^P_{i,T} = F^P_{i,L}$. As a result, the decay rates for the processes can be computed via one of the above form factors. It is advantageous to select one-loop form factors $F^P_{i,L}$ for the later analysis because these form factors do not have the ultraviolet divergent (UV-divergent). Therefore, all diagrams in Fig. 2 and Fig. 3 can be ignored in this work, as we stated previously. Hereafter, $F^P_i = F^P_{i,L}$. The one-loop form factors F^P_i are separated into two parts as follows:

$$F^P_i = \sum_{V_0 \equiv A,Z,Z'} F^P_{i,V_0^*-\text{pole}} + F^P_{i,\text{Non-pole}}, \quad \text{for} \quad i = 1,2. \tag{51}$$

The related kinematic variables for this process calculations are included as follows:

$$p^2 = M_h^2, \quad q_1^2 = q_2^2 = m_\ell^2, \quad q_3^2 = 0,$$
$$q_{12} = (q_1+q_2)^2, \quad q_{13} = (q_1+q_3)^2. \tag{52}$$

The kinematic variables also follow the relation

$$q_{12} + q_{13} + q_{23} = M_h^2 + 2m_\ell^2. \tag{53}$$

We first implement the $B-L$ models into the `FeynArt`package [65]. One-loop amplitude can be generated automatically by this package. The amplitude is then decomposed into one-loop tensor integrals. The tensor integrals are then reduced to scalar one-loop PV-functions

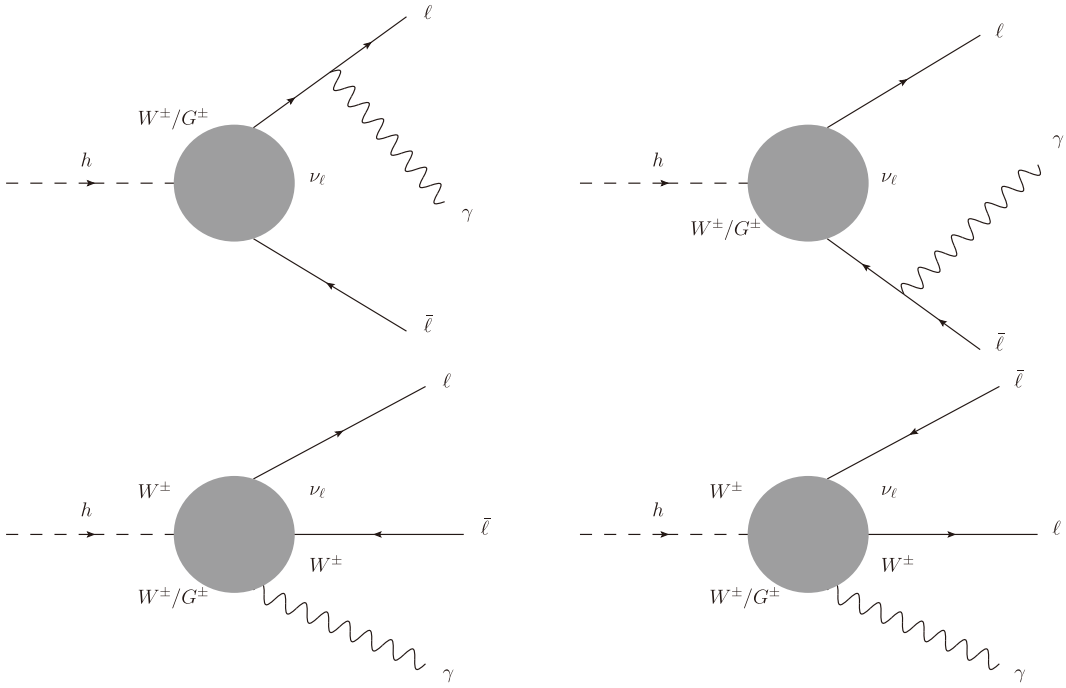

Fig. 5. One-loop Feynman non-V_0-pole diagrams with W boson exchanging in the loop.

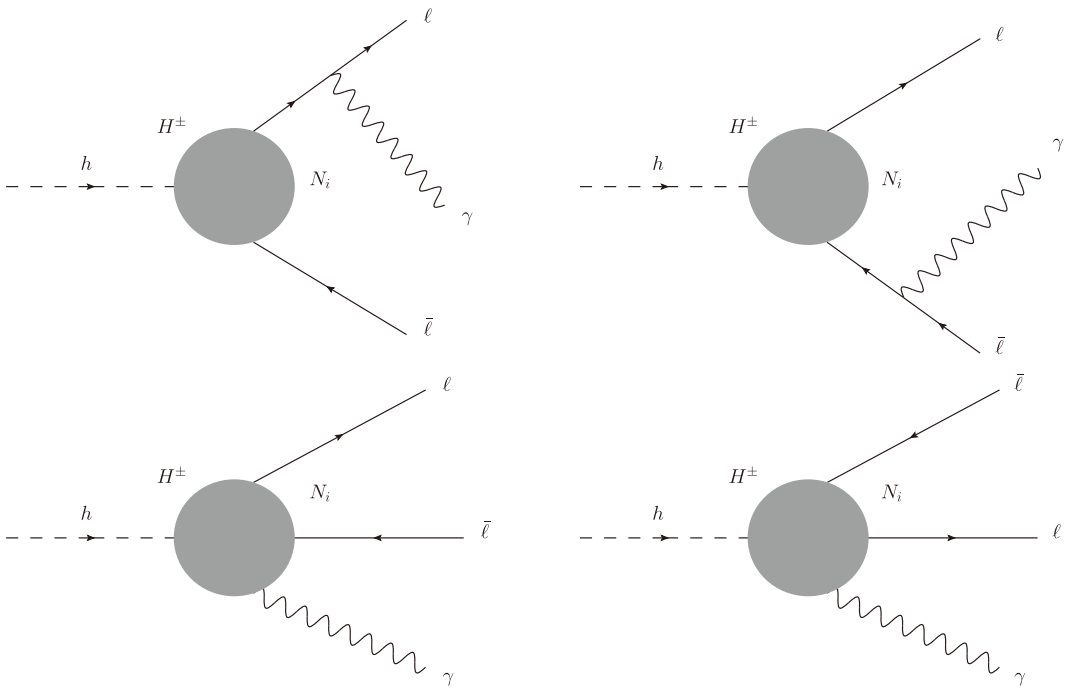

Fig. 6. One-loop Feynman non-V_0-pole diagrams with charged Higgs exchanging in the loop.

using the `FormCalc` package[66]. The one-loop form factors $F^P_{i,V_0^*-\text{pole}}$ and $F^P_{i,\text{Non}-\text{pole}}$ are collected and presented as functions of the kinematic variables $M_h^2, q_{12}, q_{13}, m_\ell^2$ and the squared internal masses. The analytical expressions for the form factors are written in terms of scalar PV-functions in the notations of `LoopTools` [67]. As a result, one-loop decay rates can be evaluated numerically by using `LoopTools`. In the next paragraphs, we show the analytical results for the form factors group by group of the Feynman diagrams.

- V_0^*-pole contributions :

We first consider all V_0^*-pole diagrams as shown in Fig. 1 including the decay of $V_0^* \to \ell\bar{\ell}$ in these diagrams. The form factors $F^P_{i,V_0^*-\text{pole}}$ can be expressed in the form of

$$F^{P}_{i,V_0^*-\text{pole}} = -\frac{\alpha}{(8\pi)M_W s_W}\frac{1}{(q_{12}-M^2_{V_0})+iM_{V_0}\Gamma_{V_0}}(g^P_{V_0^*\ell\bar{\ell}}) \times\Big\{\kappa_{hW^\pm W^\mp}\times F^{P,W^\pm}_{i,V_0^*-\text{pole}} - \sum_f \kappa_{h\bar{f}f}\left(N^C_f Q_f m^2_f\right)F^{P,f}_{i,V_0^*-\text{pole}} + F^{P,H^\pm}_{i,V_0^*-\text{pole}}\Big\} \quad (54)$$

for $P=\{L,R\}$.

From the fermions f-loop contributions, the form factor is given as follows:

$$F^{P,f}_{i,V_0^*-\text{pole}} = 4\Big(\sum_{j=L,R} g^j_{V_0^*f\bar{f}}\Big)\Big[C_0+4\big(C_2+C_{12}+C_{22}\big)\Big] \times(0,q_{12},M^2_h,m^2_f,m^2_f,m^2_f). \quad (55)$$

Here, $g^{L,R}_{V_0^*f\bar{f}}$ denotes the couplings of V_0^* with the fermion-pair in the loop. We next regard the W-boson loop contributions. This is different from our previous work in [32], where we included new parameters to unify the one-loop form factors for both the photon and Z-poles in one analytic expression. In this work, to avoid definning new parameters, we present one-loop form factors for γ^*-pole and Z^*- or Z'^*-pole separately. In detail, the form factors are shown for $V_0^*\equiv\gamma^*$-pole as follows:

$$\frac{F^{P,W^\pm}_{i,\text{A}^*-\text{pole}}}{g_{A^*WW}} = 8\Big[4M^2_W C_0+(M^2_h+6M^2_W)(C_2+C_{12}+C_{22})\Big] (0,q_{12},M^2_h,M^2_W,M^2_W,M^2_W). \quad (56)$$

Here, A^* is noted for γ^*-pole. The one form factors for $V_0^*\equiv Z^*$-pole and $V_0^*\equiv Z'^*$-pole take the form of

$$\frac{F^{P,W^\pm}_{i,V_0^*-\text{pole}}}{g_{V_0^*WW}} = 4\Big\{2M^2_W(3-t^2_W)C_0+[(M^2_h+10M^2_W) - t^2_W(M^2_h+2M^2_W)]\times \times(C_2+C_{12}+C_{22})\Big\}(0,q_{12},M^2_h,M^2_W,M^2_W,M^2_W). \quad (57)$$

Here, we have used $t_W=s_W/c_W$. In this formulas, $g_{V_0^*WW}$ shows the couplings of Z or Z' with the W-pair, which are presented in Tables 4 and 9.

In addition, the one-loop form factor with the charged Higgs bosons $H^\pm$ in the loop reads

$$F^{P,H^\pm}_{i,V_0^*-\text{pole}} = \frac{4M_W s_W}{\pi\alpha}(g_{hH^\pm H^\mp})(g_{AH^\pm H^\mp})(g_{V_0^*H^\pm H^\mp}) \times\Big[C_{12}+C_2+C_{22}\Big](0,q_{12},M^2_h,M^2_{H^\pm},M^2_{H^\pm},M^2_{H^\pm}). \quad (58)$$

Here, it is noted that $g_{V_0^*H^\pm H^\mp}$ stands for the couplings of $V_0^*H^\pm H^\mp$ with $V_0^*\equiv\gamma^*,Z^*$ and Z'^*.

We emphasize the following inportant points. First, for the case of the V_0^*-pole being γ^*- and Z^*-poles, we reduce the PV functions in Eqs. (55)–(58) to scalars one-loop functions, and then we reprodure the corresponding results in [32]. Obviously, we have to replace all the couplings factored out in all the above formulas from this model to the HESM respectively. Second, the contributions from the Z'^*-pole are new results from this work. Third, we derive alternative presentations for one-loop form factors for $h\to\ell\bar{\ell}\gamma$ in comparison with our previous work in [31], where the results are shown in the unitary gauge. Last but not least, taking the limits of V_0^* to on-shell γ or on-shell Z, we have one-loop form factors for the loop-induced $h\to\gamma\gamma$ and $h\to Z\gamma$ in the $U(1)_{B-L}$ extension of the SM.

- Non V_0-polecontributions :

We turn to one-loop diagrams without V_0-pole contributions. The form factors $F^P_{i,\text{Non-pole}}$ can be separated into the form of

$$F^P_{i,\text{Non-pole}} = \sum_{V_1,V_2\equiv\{Z,Z'\}} F^P_{i,\text{Non-pole}\,V_1,V_2} + F^P_{i,\text{Non-pole}\,W^\pm}+F^P_{i,\text{Non-pole}\,H^\pm}. \quad (59)$$

We arrive at one-loop diagrams with contributions of two neutral gauge bosons, V_1 and V_2. The form factors $F^P_{i,\text{Non-pole}\,V_1,V_2}$ are also expressed in terms of PV-functions as follows:

$$\begin{aligned}
&F^L_{1,\text{Non-pole}\,V_1,V_2}\\
&=\frac{1}{n!}\times\frac{(g_{hV_1V_2})(g^L_{A\ell\bar{\ell}})}{4\pi^2}\Big(\prod_{i=1}^{2}g^L_{V_i\ell\bar{\ell}}\Big)\times\\
&\times\Big\{[D_2+D_{12}+D_{23}](0,q_{13},M^2_h,q_{23},0,0,m^2_\ell,m^2_\ell,M^2_{V_1},M^2_{V_2})\\
&+[D_3+D_{13}+D_{23}](0,0,M^2_h,0,q_{23},q_{13},m^2_\ell,m^2_\ell,M^2_{V_1},M^2_{V_2})\Big\},\\
&F^R_{1,\text{Non-pole}\,V_1,V_2}\\
&=F^L_{1,\text{Non-pole}\,V_1,V_2}\{(g^L_{V_1\ell\bar{\ell}},g^L_{V_2\ell\bar{\ell}})\to(g^R_{V_1\ell\bar{\ell}},g^R_{V_2\ell\bar{\ell}})\},\\
&F^{L/R}_{2,\text{Non-pole}\,V_1,V_2}\\
&=F^{L/R}_{1,\text{Non-pole}\,V_1,V_2}\{q_{13}\leftrightarrow q_{23}\}.
\end{aligned} \quad (60)$$

Here, the factor $(n!)^{-1}$ denotes for two identical internal particles in the loop $(n=2)$ for the case of $V_1\equiv V_2\equiv Z$ or Z'. Next, one-loop contributions of the charged gauge bosons $W^\pm$ internal lines are considered. The form factors $F^P_{i,\text{Non-pole}\,W^\pm}$ read as follows:

$$
\begin{aligned}
&F^L_{1,\text{Non-pole}\,W^\pm}\\
&= -\frac{\alpha M_W}{\pi s_W}\kappa_{hW^\pm W^\mp}(g_{W^\pm\ell\bar{\nu}_\ell})^2\\
&\times\Big\{[D_1+D_{13}](0,q_{12},0,q_{23},0,M_h^2,m_{\ell'}^2,M_W^2,M_W^2,M_W^2)\\
&+[D_2-D_{23}-D_{33}](0,q_{12},0,q_{13},0,M_h^2,m_{\ell'}^2,M_W^2,M_W^2,M_W^2)\Big\},\\
&F^L_{2,\text{Non-pole}\,W^\pm}\\
&= F^L_{1,\text{Non-pole}\,W^\pm}\{q_{13}\leftrightarrow q_{23}\},\\
&F^R_{i,\text{Non-pole}\,W^\pm}=0.
\end{aligned}
\tag{61}
$$

We note that, in this case, $m_{\ell'}^2=m_{\nu_\ell}^2=0$ in the decay channels $h\to\ell\bar{\ell}\gamma$ and $m_{\ell'}^2=m_\ell^2\neq 0$ in the decay channels $h\to\nu_\ell\bar{\nu}_\ell\gamma$. Finally, we consider one-loop diagrams with non-pole V_0, where the charged Higgs bosons $H^\pm$and right handed neutrino N_i are exchanging in the loop.

$$
\begin{aligned}
&F^L_{1,\text{Non-pole}\,H^\pm}\\
&= -\frac{M_{N_i}^2}{8\pi^2}(g_{hH^\pm H^\mp})(g_{AH^\pm H^\mp})(g_{H^\pm\ell\bar{N}_i})^2\\
&\times\Big\{[D_2+D_{12}+D_{22}]\\
&\times(q_{12},0,q_{13},0,M_h^2,0,M_{H^\pm}^2,M_{H^\pm}^2,M_{H^\pm}^2,M_{N_i}^2)\\
&+[D_2+D_{12}+D_{22}+D_{23}]\\
&\times(q_{12},0,q_{23},0,M_h^2,0,M_{H^\pm}^2,M_{H^\pm}^2,M_{H^\pm}^2,M_{N_i}^2)\Big\},\\
&F^L_{2,\text{Non-pole}\,H^\pm}\\
&= F^L_{1,\text{Non-pole}\,H^\pm}\{q_{13}\leftrightarrow q_{23}\},\\
&F^R_{i,\text{Non-pole}\,H^\pm}=0.
\end{aligned}
\tag{62}
$$

It is important to note the following arguments. When we take only Z,W in the non-V_0-pole diagrams and replace the overall couplings respectively to the HESM, we then reprodure the corresponding results in [32]. Furthermore, including all the contributions from Z,Z',W and charged scalar Higgs in the non-V_0-pole diagrams, we derive alternative results from our previous reference [31].

Having all the one-loop form factors, we can check the calculations by verifying the UV finiteness and IR finiteness of the form factors. We verify that all the form factors presented in the calculations are UV-finite and IR-finite. As there is no virtual photon exchanging in the loop, we do not have the IR-divergence in the processes. We have confirmed the UV finiteness for the form factors analytically in [30, 32].

After confirming the correctness of the results, the differential decay rate for $h\to\ell\bar{\ell}\gamma$ including one-loop contributions can be computed as follows

$$
\begin{aligned}
\frac{\mathrm{d}\Gamma_{h\to\ell\bar{\ell}\gamma}}{\mathrm{d}q_{12}\,\mathrm{d}q_{13}} &= \frac{q_{12}}{512\pi^3M_h^2}\Big[q_{13}^2\Big(\left|F_1^L\right|^2+\left|F_1^R\right|^2\Big)\\
&+q_{23}^2\Big(\left|F_2^L\right|^2+\left|F_2^R\right|^2\Big)\Big].
\end{aligned}
\tag{63}
$$

After integrating over $(m_{\ell\bar{\ell}}^{\text{cut}})^2\le q_{12}\le M_h^2$ and $0\le q_{13}\le M_h^2-q_{12}$, one then obtains the total decay rates. At the LHC, the signal strengths for $h\to\ell\bar{\ell}\gamma$ can be derived as follows:

$$
\mu_{B-L}=\frac{\sigma^{B-L}(pp\to h)}{\sigma^{SM}(pp\to h)}\frac{\Gamma^{B-L}_{h\to\ell\bar{\ell}\gamma}}{\Gamma^{SM}_{h\to\ell\bar{\ell}\gamma}}\frac{\Gamma^{SM}_{h\to\text{all}}}{\Gamma^{B-L}_{h\to\text{all}}}.
\tag{64}
$$

Here, $\Gamma^{B-L}_{h\to\text{all}}=\Gamma^{SM}_{h\to\text{all}}+\Gamma^{B-L}[h\to Z'Z']+\Gamma^{B-L}[h\to\sum_{i=1}^{3}N_i\bar{N}_i]$. In the scenario of a heavy neutral gauge boson Z' and heavy neutrinos N_i ($M_{N_i}\sim 1$ TeV), we then confirm that $\Gamma^{B-L}_{h\to\text{all}}\simeq\Gamma^{SM}_{h\to\text{all}}$. Furthermore, we verify that

$$
\frac{\sigma^{B-L}(pp\to h)}{\sigma^{SM}(pp\to h)}\simeq\kappa_{hff}^2.
\tag{65}
$$

Here, κ_{hff} is defined as in Eq. (49). Therefore, the signal strengths can be evaluated as

$$
\mu_{B-L}\simeq\kappa_{hff}^2\times\frac{\Gamma^{B-L}_{h\to\ell\bar{\ell}\gamma}}{\Gamma^{SM}_{h\to\ell\bar{\ell}\gamma}}.
\tag{66}
$$

In the scope of this work, we are interested in this limit and take the signal strengths in Eq. (66) for the phenomenological analysis at the LHC.

B. Form factors for $e^-e^+\to h\gamma$

We turn our attention to evaluate cross-sections for $e^-e^+\to h\gamma$ at future LCs. Applying the same method for $h\to\ell\bar{\ell}\gamma$, the one-loop amplitude for the production process can be written in terms of the following Lorentz structure :

$$
\begin{aligned}
\mathcal{A}^{e^-e^+\to h\gamma}_{1-\text{loop}} &= \sum_{i=\{1,2\}}\sum_{P=\{L,R\}}\Big\{\bar{v}(q_2)\Big(\gamma_\nu O_P\Big)K_i^P\\
&\times\Big[q_i^\mu q_3^\nu-\Big(q_i\cdot q_3\Big)g^{\mu\nu}\Big]u(q_1)\Big\}\varepsilon_\mu^*(q_3).
\end{aligned}
\tag{67}
$$

Here, the one-loop form factors K_i^P are collected as coefficient of $q_i^\mu q_3^\nu$. By comparing with the one-loop form factors F_i^P, we find that the form factors K_i^P can be derived from F_i^P by applying the following relations:

$$
K^P_{i,V_0^*-\text{pole}}=F^P_{i,V_0^*-\text{pole}};
\tag{68}
$$

$$
K^P_{i,\text{Non-pole}}=F^P_{i,\text{Non-pole}}\,|_{q_{13}\leftrightarrow q_{23}}\quad\text{for } P=L,R.
\tag{69}
$$

The above relations can be explained by applying cross-symmetry for converting the decay process $h \to e^-e^+\gamma$ to the production scattering $e^-e^+ \to h\gamma$; see [63] for more detail. The differential cross section for the production process, including initial beam polarizations, can be expressed in terms of one-loop form factors as follows:

$$\frac{d\sigma_{\rm pol}}{d\cos\theta_{e^-\gamma}} = \frac{q_{12}-M_h^2}{256\pi q_{12}}\Big\{\big(1+\lambda_+\big)\big(1-\lambda_-\big)\big[q_{13}^2|F_1^L|^2+q_{23}^2|F_2^L|^2\big] + \big(1-\lambda_+\big)\big(1+\lambda_-\big)\big[q_{13}^2|F_1^R|^2+q_{23}^2|F_2^R|^2\big]\Big\} \tag{70}$$

where λ_- and λ_+ are the polarized degrees of the initial e^- and e^+ beams, respectively. In the above expression, q_{23}, q_{13} are given by

$$q_{23}, q_{13} = -\frac{q_{12}-M_h^2}{2}\big(1\mp\cos\theta_{e^-\gamma}\big). \tag{71}$$

Here, $\theta_{e^-\gamma}$ is the angle between the initial electron and external photon.

The signal strengths for the Higgs production associated with a photon for the models at future LCs can be estimated as follows:

$$\mu_{B-L}(\sqrt{s},\lambda_+,\lambda_-) = \frac{\sigma_{B-L}}{\sigma_{SM}}(\sqrt{s},\lambda_+,\lambda_-). \tag{72}$$

Here, $\sqrt{s}$ is center-of-mass energy. In the next section, we present the phenomenological results for the calculations.

IV. PHENOMENOLOGICAL RESULTS

In the phenomenological results, we use the following input parameters: $M_Z = 91.1876$ GeV, $\Gamma_Z = 2.4952$ GeV, $M_W = 80.379$ GeV, $\Gamma_W = 2.085$ GeV, $M_h = 125$ GeV, and $\Gamma_H = 4.07\cdot 10^{-3}$ GeV. The lepton masses are selected as $m_e = 0.00052$ GeV, $m_\mu = 0.10566$ GeV, and $m_\tau = 1.77686$ GeV. For quark masses, one takes $m_u = 0.00216$ GeV, $m_d = 0.0048$ GeV, $m_c = 1.27$ GeV, $m_s = 0.93$ GeV, $m_t = 173.0$ GeV, and $m_b = 4.18$ GeV. We work in the so-called G_μ-scheme in which the Fermi constant is taken as $G_\mu = 1.16638\cdot 10^{-5}$ GeV^{-2} and the electroweak coupling can be calculated appropriately as follows:

$$\alpha = \sqrt{2}/\pi G_\mu M_W^2(1-M_W^2/M_Z^2) = 1/132.184. \tag{73}$$

As we show later in this paper, the mass of the Z' boson is considered as a parameter. The total decay width of Z' can be calculated as in [68]. As indicated in the previous sections, the models $B-L$ contain an additional neutral gauge boson Z' associated with the coupling $g_X = g_{B-L}$ in the gauge sector. The limit on $M_{Z'}$ and g_{B-L} reported by Tevatron [69] is

$$\frac{M_{Z'}}{2g_{B-L}} \gtrsim 3\ \text{TeV}. \tag{74}$$

Moreover, from the electroweak precision test (EWPT) [70, 71], one has the further constraint on the $M_{Z'}-g_{B-L}$ parameter space as follows:

$$\frac{M_{Z'}}{2g_{B-L}} \gtrsim 3.5\ \text{TeV}. \tag{75}$$

In the LHC era, we can probe Z' via the processes $pp \to Z' \to l\bar{l}$. Recently, ATLAS [72] and CMS [73] reported a lower bound of $M_{Z'}$, $M_{Z'} \gtrsim 4.8$ GeV. In the scalar sector, $B-L$ models include the neutral Higgs H and mixing angle $\sin\theta$ of the SM-like Higgs with a scalar singlet χ. According to the results from LHC run II data in [74–77], we have the limits $|\sin\theta| < 0.37$ for 150 GeV $\le M_H \le 1000$ GeV. We also have two heavy neutrinos N_i in the neutrino sector. Direct searches for heavy neutrinos can be performed at LCs via channels $e^-e^+ \to N_i\nu$, where $N_i \to lW, \nu Z, \nu h$, *etc*. At LEP and LEP II [78, 79], the limits for M_{N_i} are 10 GeV $\le M_{N_i} \le 80$ GeV. At the LHC [80–85], heavy neutrinos mixing to light neutrinos can be probed via processes such as $pp \to W^{\pm,*} \to Nl^\pm \to l^\pm l^\pm jj$. The data present the limits on M_{N_i} as 1 GeV $\le M_{N_i} \le 1000$ GeV.

A. Numerical checks confirming gauge invariance

We first confirm the results of the decay rates of $h \to \ell\bar{\ell}\gamma$ in vector $B-L$ in our previous work [31], in which the computations were performed in the unitary gauge. We use the same input parameters as in [31]. The cross-check results are listed in Table 12. In the first column, we apply the cuts $m_{e^-e^+}^{\rm cut} = k^{\rm cut}M_h$ and $E_\gamma^{\rm cut}$, the same as in [31]. As a result, the integration region is now $(m_{e^-e^+}^{\rm cut})^2 \le q_{12} \le M_h^2(1-2E_\gamma^{\rm cut})$ and $(m_{e^-e^+}^{\rm cut})^2 \le q_{13} \le M_h^2 - q_{12}$. The second column lists the results from this work in the HF gauge. The last column presents the results in [31]. We find that the two results are good agreement. The checks confirm gauge invariance: the results remain unchanged in the different gauges.

We then cross-check the cross sections for $e^-e^+ \to h\gamma$ in this work with those of previous computations within the SM. The results for this test are presented in Table 13. In the first column, we select polarized degrees for initial beams of electron and positron. The second column lists the results from this work. The results in the last column are from Ref. [86]. Both sets of results are in good agreement, up to the last digits. The effects of one-loop contributing to the differential decay rates of $h \to \bar{l}l\gamma$ in the

Table 12. Decay rate (in KeV) $\Gamma_{h\to\ell\bar{\ell}\gamma}$ for $U(1)_{B-L}$ non-mixing in unitary and HF gauges. Here, $m^{\rm cut}_{e^-e^+}=k^{\rm cut}M_h$, considering the case of $c_\theta=0.98, g'=10^{-3}$, and $M_{Z'}=10$ GeV. The energy cut for the external photon is presented in GeV.

$(k^{\rm cut},E^{\rm cut}_\gamma)$	This work	Ref. [31]
(0.05, 1)	0.265513	0.265498
(0.1, 5)	0.239109	0.239101
(0.2, 10)	0.198871	0.198859
(0.3, 15)	0.160219	0.160212
(0.4, 20)	0.122837	0.122831

Table 13. Numerical results in femtobarn (fb) from cross-checking the cross section $\sigma_{\rm pol}$ with various different beam polarizations (λ_-,λ_+) at CMS energy $\sqrt{s}=250$ GeV, compared with the numerical values (P_{e^-},P_{e^+}) in Table 1 in Ref. [86] within the framework of the Standard Model.

(λ_-,λ_+)	This work	Ref. [86]
$(-100\%,+100\%)$	0.34999	0.35
$(+100\%,-100\%)$	0.01591	0.016
$(-80\%,+30\%)$	0.20234	0.20

vector $B-L$ model were presented in [31]. In this work, we focus on the signal strengths $h\to\ell\bar{\ell}\gamma$ in both the vector and chiral $B-L$models at the LHC. Moreover, we also examine the signal strengths for the Higgs production associated with a photon for the models at future LCs.

B. Decay process $h\to\ell\bar{\ell}\gamma$ at the LHC

We arrive at the phenomenological results for the decay process $h\to\ell\bar{\ell}\gamma$ at the LHC in the vector and chiral $B-L$ models. The signal strengths given in (66) are examined in the following subsections.

1. *Vector $B-L$ model*

In the vector $B-L$ model, new physical parameters are included: mixing angle between two neutral Higgses (c_θ), $U(1)_{B-L}$ coupling $g_X=g_{B-L}$, a new neutral gauge boson M'_Z, the kinematic mixing parameter κ, and the mixing angle (s_{BL}) of the two gauge bosons Z and Z'. For the numerical results in this section, we only consider the non-mixing gauge bosons (non-mixing between two $U(1)$ gauges) in which we apply the limits of $\kappa\to 0, s_{BL}\to 0$.

In Fig. 7, the signal strengths are generated as functions of c_θ and M'_Z . In this plot, we set $g_{B-L}=0.07$. By considering experimental constraints such as $\frac{M'_Z}{2g_{B-L}}\geq 3.5$ TeV, the mass of the neutral gauge boson $M'_Z\geq 490$ GeV. For this reason, the signal strengths are shown in the ranges of 490 GeV $\leq M'_Z\leq 1000$ GeV. The mixing angle of two neutral Higgses is taken as $0.85\leq c_\theta\leq 0.98$. We

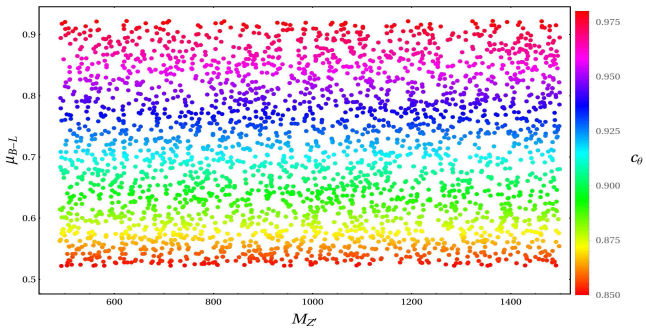

Fig. 7. (color online) Signal strengths for the decay process in vector $B-L$ shown as functions of c_θ and M'_Z at the LHC.

find that the signal strengths are proportional to the mixing angle and depend slightly on M'_Z. This shows that the contributions of the neutral gauge boson Z' are rather small. The effects of the neutral gauge boson Z' on the decay rates for the processes are difficult to probe at the LHC.

2. *Chiral $B-L$ model*

In this version of $B-L$, together with the g_{B-L},M'_Z mixing angle (s'_{BL}) of two gauge bosons of $U(1)$ gauge groups, we include three more mixing angles of neutral Higgses as c_{12},c_{13},c_{23}, mixing angle of charged Higgs with charged Goldstone boson t_α, and mixing angle between neutral Goldstone bosons and CP-odd Higgs t_β. The masses of the new particles in this version are $M_{H_{2,3}},M_{A_0},M_{H^\pm},M_{N_i}$. For the numerical results, considering the non-mixing gauge boson case (or $s'_{BL}\to 0$), we also take the simplest case as $c_{13}=c_{23}=1$. The mixing angle between H_1 (treated as SM-like Higgs boson) and H_2 is $c_{\widehat{12}}$. In this limit, the coupling of hH^+H^- is then derived as follows:

$$g_{hH^+H^-}=\frac{1}{v}\Big\{\Big[-\frac{\sqrt{2}\mu v_\sigma}{s_\alpha c_\alpha}+2M^2_{H^\pm}-M^2_h\Big]c_{\alpha+\widehat{12}} + \Big[\frac{\sqrt{2}\mu v_\sigma}{s_\alpha c_\alpha}\cot(2\alpha)\,s_{\alpha+\widehat{12}}+\frac{M^2_h}{s_\alpha c_\alpha}s_{\alpha-\widehat{12}}\Big]\Big\}. \quad (76)$$

In this model, we have $\kappa_{hVV}=c_{\alpha+\widehat{12}}$. For the phenomenological studies, we are interested in the the case (the SM limit) $c_{\alpha+\widehat{12}}\to 1$.

In Fig. 8, the signal strengths are presented as functions of t_α and charged Higgs mass $M_{H^\pm}$. The values of μ_{B-L} are generated in the ranges of $3\leq t_\alpha\leq 20$ and 600 GeV $\leq M_{H^\pm}\leq 1500$ GeV. One selects $g_{B-L}=0.005$, $M'_Z=500$ GeV, and masses of right handed neutrinos $M_{N_i}\sim O(1)$ TeV. Furthermore, $v_\sigma=3.5$ TeV and in combination with the values of $v\sim 246$ GeV and t_α, we then obtain v_Φ and v_ϕ. Having the value of v_σ, and taking $M_{A_0}=800$ GeV, the value of μ can be then obtained appropriately (follows Eq. (37)). In principle, $-\pi/2\leq$

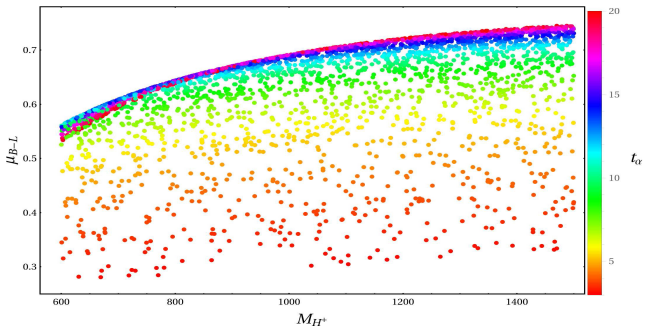

Fig. 8. (color online) Signal strengths for the decay process in chiral $B-L$ shown as functions of t_α and charged Higgs mass $M_{H^\pm}$ at the LHC.

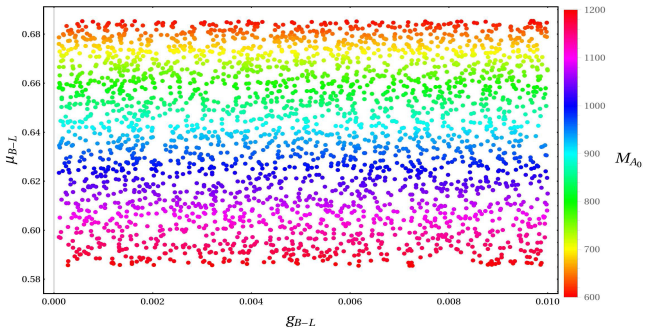

Fig. 9. (color online) Signal strengths for the decay process in chiral $B-L$ shown as functions of g_{B-L} and CP-odd Higgs mass M_{A_0} at the LHC. The vertical grey line is shown in this Figure for distinguishing from the plotting boundary.

$\widehat{12} \le \pi/2$. As mentioned above, we are interested in the SM limit $c_{\alpha+\widehat{12}} \to 1$. For example, one takes $c_{\alpha+\widehat{12}} = 0.95$ for the following plot. In this plot, we find that the signal strengths are increased with a developing $M_{H^\pm}$. At a fix value of $M_{H^\pm}$, μ_{B-L} is also proportional to t_α. The scatter plot shows that the contributions from charged Higgs to the processes are significant and the effects can be probed at the HL-LHC.

We are particularly interested in the contributions of the CP-odd Higgs to the signal strengths. In Fig. 9, the signal strengths are presented as functions of g_{B-L} and CP-odd Higgs mass M_{A_0} at the LHC. For the scatter plot, we take $t_\alpha = 10$, $M_{H^\pm} = 1000$ GeV, and $M'_Z = 500$ GeV. The values of μ_{B-L} are generated in the ranges of $10^{-4} \le g_{B-L} \le 10^{-2}$ and 600 GeV $\le M_{A_0} \le$ 1200 GeV. The masses of the right handed neutrinos are selected as $M_{N_i} \sim O(1)$ TeV and the mixing angle is taken as $c_{\alpha+\widehat{12}} = 0.95$ for the following plot. We find that the signal strengths depend significantly on M_{A_0} but change slightly with g_{B-L}. This shows that the contribution from Z' is rather small in comparison with those from chiral Higgs scalars. The indirect impacts of M_{A_0} on the signal strengths can be explained as follows. By changing M_{A_0}, the values of μ in Eq. (37) are varied appropriately. This leads to the change in the coupling $hH^\pm H^\mp$ in Eq. (76). This fact explains that the signal strengths change crucially with M_{A_0}.

C. Process $e^-e^+ \to h\gamma$ at future lepton colliders

We turn to Higgs production associated with a photon at future LCs within vector and chiral $B-L$ versions.

1. *Vector $B-L$ model*

As in previous cases, we also consider the non-mixing gauge bosons, $\kappa \to 0, s_{BL} \to 0$, for the following numerical results. In Figs. 10, 11, the signal strengths as functions of c_θ and M'_Z are presented at $\sqrt{s} = 250$ GeV and at $\sqrt{s} = 500$ GeV, respectively. In these plots, we take the same previous input parameters, that is, $g_{B-L} = 0.07$, 490 GeV $\le M'_Z \le$ 1000 GeV, and $0.85 \le c_\theta \le 0.98$. In the left panel, we show the signal strengths in the LR polarization case ($e^-_L e^+_R$), whereas those in the RL polarization case ($e^-_R e^+_L$) are presented in the right panel.

At $\sqrt{s} = 250$ GeV, we find that the signal strengths are proportional to the mixing angle c_θ and change slightly with M'_Z. The plots indicate that the contributions from Z' are rather small. As a result, the effects of Z' to the decay processes are difficult to probe at future LCs. At $\sqrt{s} = 500$ GeV, around the Z'-peak, $\sqrt{s} = M'_Z \sim$ 500 GeV, we also find the peak of the signal strengths. Beyond the M'_Z-peak region, the same behavior of signal strengths as in a previous case is observed: the signal strengths are proportional to the mixing angle c_θ and change slightly with M'_Z. It is indicated that the contributions from Z' are rather small beyond the Z'-peak. Consequently, the impacts of Z' on the decay rates for the processes are difficult to measure at future LCs. One may probe the contributions of Z' to μ_{B-L} around the Z'-peak at future LCs.

2. *Chiral $B-L$ model*

In Fig. 12 (and Fig. 13), the signal strengths are presented as functions of t_α and charged Higgs mass $M_{H^\pm}$ at $\sqrt{s} = 250$ GeV ($\sqrt{s} = 500$ GeV), respectively. In these plots, the values of μ_{B-L} are generated in the ranges of $3 \le t_\alpha \le 20$ and 600 GeV $\le M_{H^\pm} \le$ 1500 GeV. Further, one selects $g_{B-L} = 0.005$, $M'_Z = 500$ GeV, masses of right handed neutrinos $M_{N_i} = 10$ GeV, and $M_{A_0} = 800$ GeV. As mentioned above, we are also interested in the SM limit $c_{\alpha+\widehat{12}} \to 1$. For example, one takes $c_{\alpha+\widehat{12}} = 0.95$ for the following plots.

The left and right panels show the signal strengths for the LR and RL polarization cases, respectively. By implying the initial beam polarizations, there are no contributions of one-loop non V_0-pole diagrams with exchanging W boson and charged Higgs in the loop for the RL case (see Figs. 5, 6). This explains the different behavior of μ_{B-L} in the LR and RL cases. This also explains why the values of μ_{B-L} in the RL case are bigger than those in the

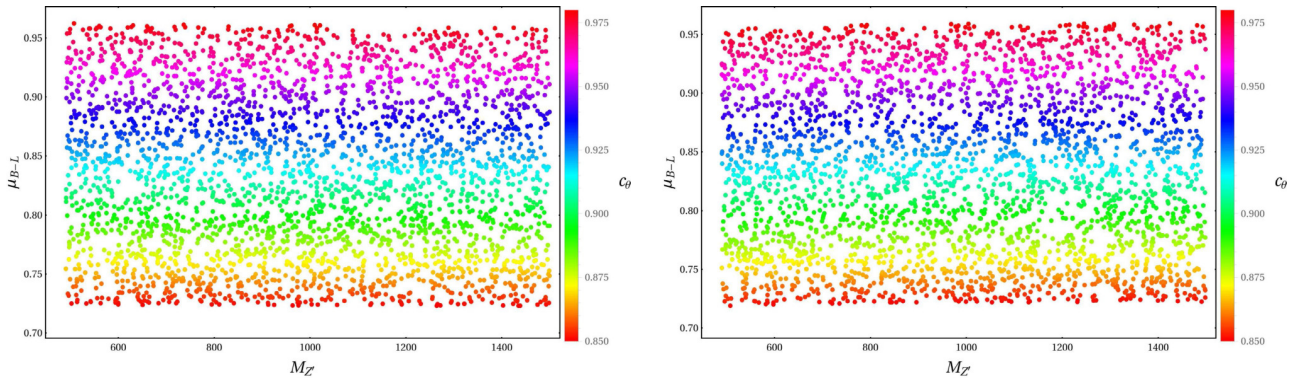

Fig. 10. (color online) Signal strengths for the process $e^-e^+ \to h\gamma$ in the vector $B-L$ model at a center-of-mass energy $\sqrt{s} = 250$ GeV. The left panel shows the LR polarization case, and the right panel presents the RL polarization case.

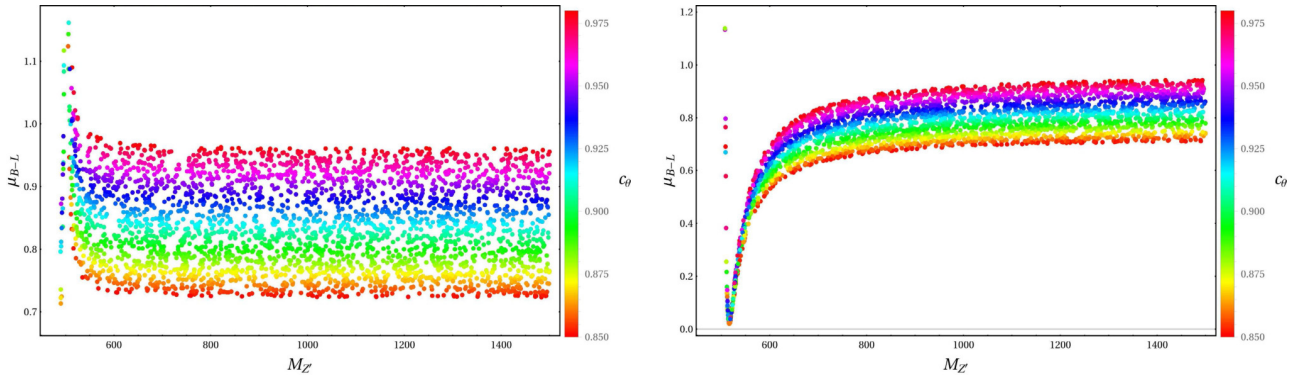

Fig. 11. (color online) Signal strengths for the process $e^-e^+ \to h\gamma$ in the vector $B-L$ model at a center-of-mass energy $\sqrt{s} = 500$ GeV. The left panel shows the LR polarization case, and the right panel presents the RL polarization case. The horizontal grey line appears for distinguishing from the boundary of the right scatter plot.

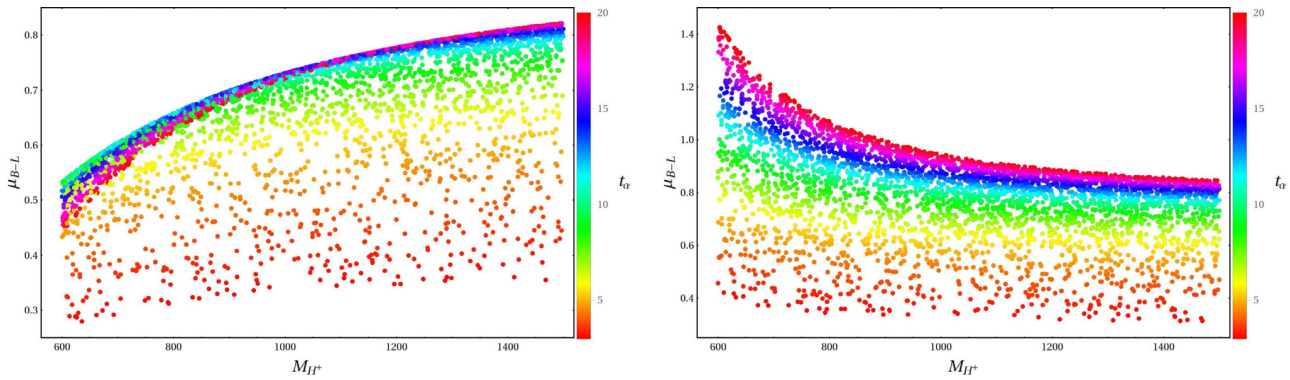

Fig. 12. (color online) Signal strengths for the process $e^-e^+ \to h\gamma$ in the chiral $B-L$ model at $\sqrt{s} = 250$ GeV. The left panel presents the LR polarization case, and the right panel shows the RL polarization case.

LR case. Moreover, it is interesting to find that the signal strengths increase with the charged Higgs mass in the LR case, while μ_{B-L} decrease with the charged Higgs mass in the RL case. The signal strengths μ_{B-L} are also sensitive to t_α at the fix value of the charged Higgs mass. The results show that the effects of charged Higgs bosons in the loop are significant in comparison with the those from Z' in $U(1)_{B-L}$. From the scatter plots, one can probe the charged Higgs contributions via the production process at future LCs.

In Fig. 14 (and Fig. 15), the signal strengths are shown as functions of t_α and right handed neutrino mass M_{N_i}. In these plots, we present μ_{B-L} in the ranges of $3 \le t_\alpha \le 20$ and 1 GeV $\le M_{N_i} \le 150$ GeV. We take $g_{B-L} = 0.005$, $M'_Z = 500$ GeV, and charged Higgs mass $M_{H^\pm} = 1000$ GeV. As in the previous case, having $v_\sigma = 3.5$ TeV and $M_{A_0} = 800$ GeV, the value of μ can be then derived appropriately. We are also very interested in the SM lim-

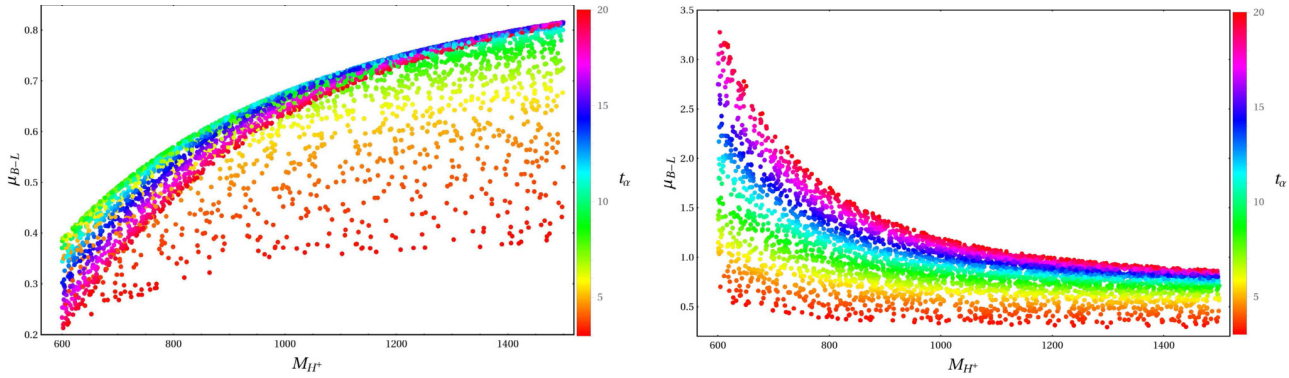

Fig. 13. (color online) Signal strengths for the process $e^-e^+ \to h\gamma$ in the chiral $B-L$ model at $\sqrt{s} = 500$ GeV. The left panel presents the LR polarization case, and the right panel shows the RL polarization case.

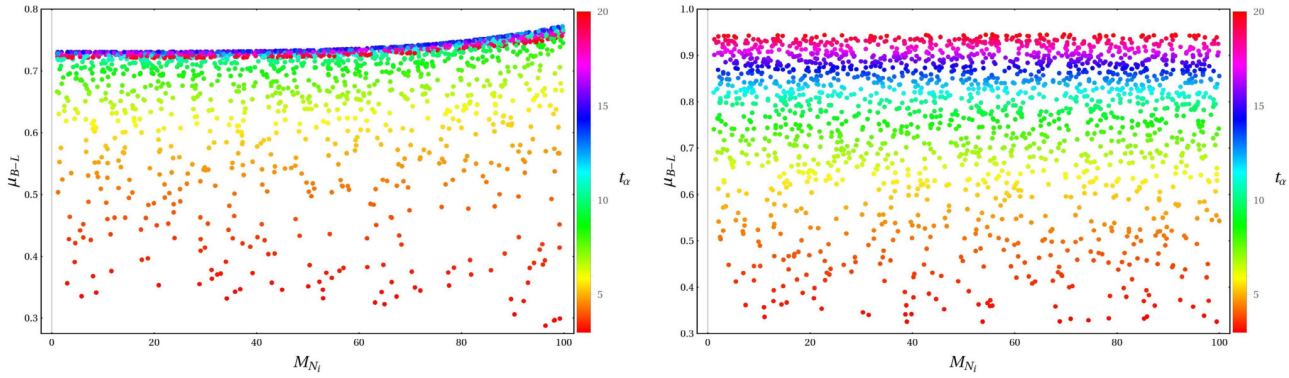

Fig. 14. (color online) Signal strengths for the process $e^-e^+ \to h\gamma$ in the chiral $B-L$ model at $\sqrt{s} = 500$ GeV. The left panel presents the LR polarization case, and the right panel shows the RL polarization case. The vertical grey lines appear in the Figure for distinguishing from the plotting boundary.

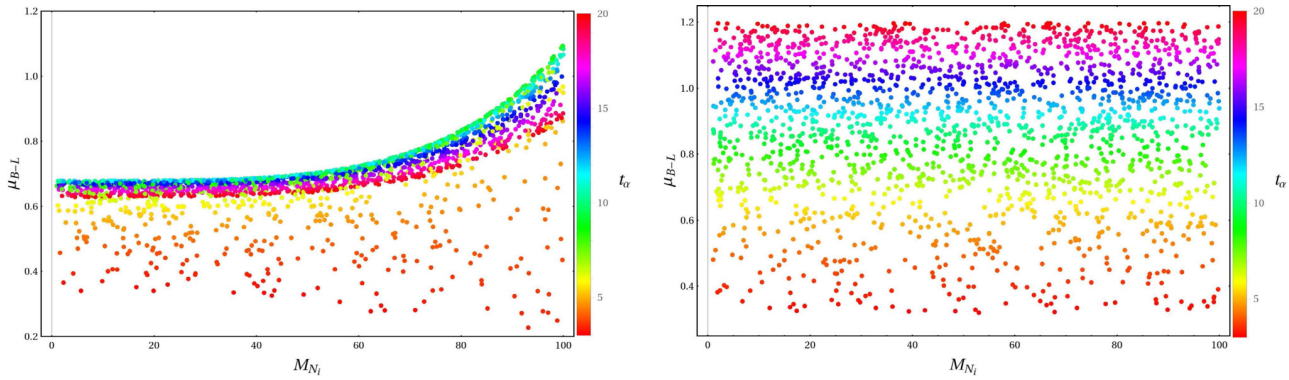

Fig. 15. (color online) Signal strengths for the process $e^-e^+ \to h\gamma$ in the chiral $B-L$ model at $\sqrt{s} = 500$ GeV. The left panel presents the LR polarization case, and the right panel shows the RL polarization case. The vertical and horizontal grey lines appear in the Figures for distinguishing from the plotting boundary.

it $c_{\alpha+\widehat{12}} \to 1$ and take, for example, $c_{\alpha+\widehat{12}} = 0.95$ in these plots. In the left panel, we have signal strengths for the LR polarization case, whereas the right panel shows the signal strengths for the RL polarization case. We find that the signal strengths are unchanged in the case of RL polarization because there are no contributions from the charged Higgs box diagrams. As a result, μ_{B-L} must be unchanged with varying M_{N_i}. In the left panel, the signal strengths depend slightly on M_{N_i} at $\sqrt{s} = 250$ GeV. One finds more impacts of M_{N_i} on signal strengths at $\sqrt{s} = 500$ GeV.

As in previous discussions, we also consider of interest the contributions of M_{A_0} to the signal strengths at future LCs. In Figs. 16, 17, the signal strengths are shown as functions of g_{B-L} and M_{A_0} at $\sqrt{s} = 250$ GeV and $\sqrt{s} = 500$ GeV, respectively. In these Figures, we set the

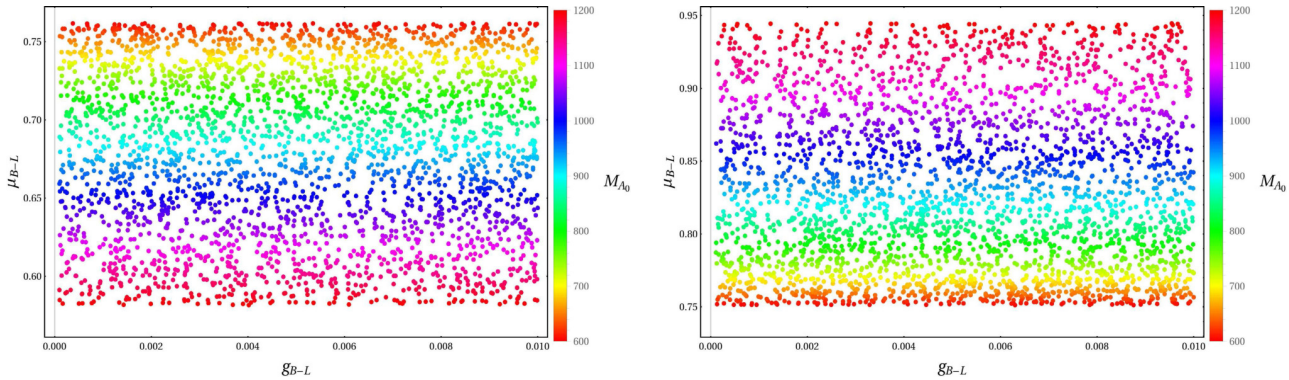

Fig. 16. (color online) Signal strengths for the production process in the chiral $B-L$ shown as functions of g_{B-L} and CP-odd Higgs mass M_{A_0} at $\sqrt{s}=250$ GeV at future LCs. The left panel presents the LR polarization case, and the right panel shows the RL polarization case. The vertical grey lines in the Figures appear for distinguishing from the plotting boundary.

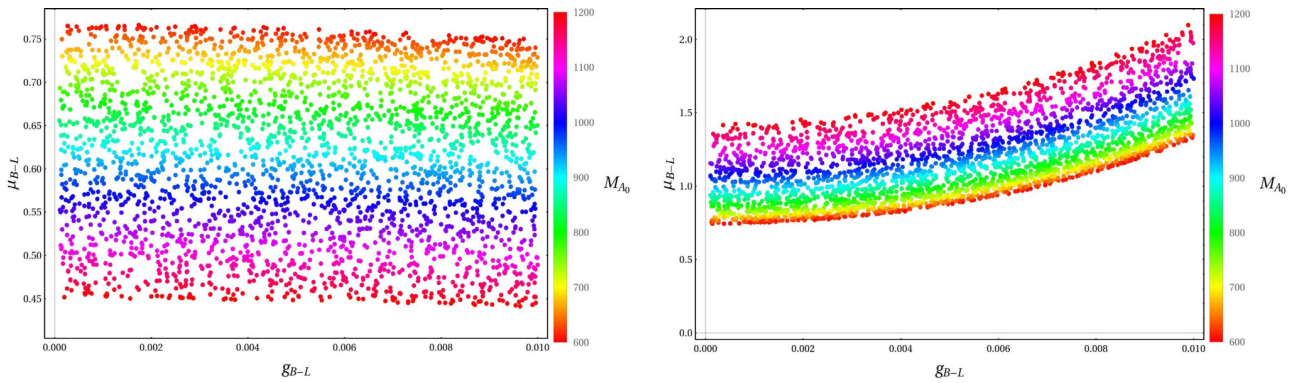

Fig. 17. (color online) Signal strengths for the production process in chiral $B-L$ shown as functions of g_{B-L} and M_{A_0} at $\sqrt{s}=500$ GeV at future LCs. The left panel presents the LR polarization case, and the right panel shows the RL polarization case. The vertical and horizontal grey lines appear in the Figures for distinguishing from the boundary of the scatter plots.

following parameters as $t_\alpha=10$, $M_{H^\pm}=1000$ GeV, and $M'_Z=500$ GeV. Furthermore, the values of μ_{B-L} are generated in the regions of $10^{-4}\le g_{B-L}\le 10^{-2}$ and 600 GeV $\le M_{A_0}\le 1200$ GeV. The masses of right handed neutrinos are selected as $M_{N_i}=10$ GeV, and the mixing angle is taken as $c_{\alpha+\widehat{12}}=0.95$ for the following plots. At $\sqrt{s}=250$ GeV, the signal strengths depend significantly on M_{A_0} but change slightly with g_{B-L}. This shows that the contribution from Z' is rather small in comparison with the contributions from chiral Higgs scalars. In the LR polarization case at $\sqrt{s}=500$ GeV, we observe the same behavior of μ_{B-L} as that in the previous cases at $\sqrt{s}=250$ GeV. At high energy regions, the attribution from Z' in the loop has more impact on the decay rates because we only consider the non-mixing of Z and Z'. Subsequently, there is no Z'-pole with the W-loop in this case. Futhermore, the contributions of box diagrams with Z' exchanging in the loop are much smaller in comparison with those with the W boson loop. This explains why μ_{B-L} depend slightly on g_{B-L} in this case. It is interesting to find that the signal strengths change significantly for both M_{A_0} and g_{B-L} in the RL polarized case at $\sqrt{s}=500$ GeV. With the absence of the W-boson, and charged Higgs in the loop diagrams, the box diagrams with the Z' internal lines contribute to μ_{B-L} with more substantial effects. The signal strengths depend crucially on g_{B-L} at fixing M_{A_0}.

V. CONCLUSIONS

In this work, we presented one-loop form factors for $h\to\ell\bar{\ell}\gamma$ in the $U(1)_{B-L}$ extension of the SM. The computations were performed in the 't Hooft-Feynman gauge. We showed that the production cross-sections for $e^-e^+\to h\gamma$ at future LCs can be derived by using one-loop form factors in the decay $h\to\ell\bar{\ell}\gamma$. The form factors are expressed in terms of one-loop scalar PV-functions in the standard notation of `LoopTools`. As a result, the one-loop decay rates, cross-sections, and signal strengths can be evaluated numerically by using `LoopTools`. In the phenomenological results, the signal strengths for $h\to\ell\bar{\ell}\gamma$ at the LHC and for $e^-e^+\to h\gamma$ at future LCs were investigated in the physical parameter space for both the vector and chiral $B-L$ models. We find that the contributions from the neutral gauge boson Z' to the signal strengths are rather small. Consequently, the effects from Z' in the models are difficult to probe at future colliders, whereas

the impacts of charged Higgs in the chiral $B-L$ model on the signal strengths are significant and can be measured with the help of the initial polarization beams at future LCs.

ACKNOWLEDGMENT

Dzung Tri Tran and Khiem Hong Phan express their gratitude for the valuable support from Duy Tan University in the 30th anniversary of its establishment (Nov. 11, 1994 - Nov. 11, 2024) aimed at "Integral, Sustainable, and Stable Development".

APPENDIX A: PV-FUNCTIONS AND CHECKS FOR THE CALCULATIONS

We follow the approach in [87] for tensor reductions for one-loop integrals. Based on the method, tensor one-loop integrals with N-external lines can be expressed in terms of a scalar one-loop with one-, two-, three-, and four-point functions. The definition for tensor one-loop integrals with rank R is as follows (up to four point functions):

$$\{A;B;C;D\}^{\mu_1\mu_2\cdots\mu_R} = (\mu^2)^{2-d/2} \times \int \frac{d^dk}{(2\pi)^d} \frac{k^{\mu_1}k^{\mu_2}\cdots k^{\mu_R}}{\{P_1;P_1P_2;P_1P_2P_3;P_1P_2P_3P_4\}} \tag{A1}$$

In this formula, P_j^{-1} $(j=1,\cdots,4)$ are Feynman propagators

$$P_j = (k+q_j)^2 - m_j^2 + \mathrm{i}\epsilon. \tag{A2}$$

The momenta $q_j = \sum_{i=1}^{j} p_i$ are taken into account where external momenta p_j and internal masses m_j are involved. The term $i\epsilon$ is a Feynman prescription. Space-time dimension d takes the form of $d=4-2\varepsilon$ with $\varepsilon \to 0$ at the final results. The parameter μ^2 is an overall factor of tensor integrals playing role of a renormalization scale. The reduction formulas for tensor one-loop one-, two-, three-, and four-point integrals up to the rank $R=3$ are as follows [87]:

$$A^\mu = 0, \tag{A3}$$

$$A^{\mu\nu} = g^{\mu\nu}A_{00}, \tag{A4}$$

$$A^{\mu\nu\rho} = 0, \tag{A5}$$

$$B^\mu = q^\mu B_1, \tag{A6}$$

$$B^{\mu\nu} = g^{\mu\nu}B_{00} + q^\mu q^\nu B_{11}, \tag{A7}$$

$$B^{\mu\nu\rho} = \{g,q\}^{\mu\nu\rho}B_{001} + q^\mu q^\nu q^\rho B_{111}, \tag{A8}$$

$$C^\mu = q_1^\mu C_1 + q_2^\mu C_2 = \sum_{i=1}^{2} q_i^\mu C_i, \tag{A9}$$

$$C^{\mu\nu} = g^{\mu\nu}C_{00} + \sum_{i,j=1}^{2} q_i^\mu q_j^\nu C_{ij}, \tag{A10}$$

$$C^{\mu\nu\rho} = \sum_{i=1}^{2}\{g,q_i\}^{\mu\nu\rho}C_{00i} + \sum_{i,j,k=1}^{2} q_i^\mu q_j^\nu q_k^\rho C_{ijk}, \tag{A11}$$

$$D^\mu = q_1^\mu D_1 + q_2^\mu D_2 + q_3^\mu D_3 = \sum_{i=1}^{3} q_i^\mu D_i, \tag{A12}$$

$$D^{\mu\nu} = g^{\mu\nu}D_{00} + \sum_{i,j=1}^{3} q_i^\mu q_j^\nu D_{ij}, \tag{A13}$$

$$D^{\mu\nu\rho} = \sum_{i=1}^{3}\{g,q_i\}^{\mu\nu\rho}D_{00i} + \sum_{i,j,k=1}^{3} q_i^\mu q_j^\nu q_k^\rho D_{ijk}. \tag{A14}$$

Tensor $\{g,q_i\}^{\mu\nu\rho}$ is defined as follows: $\{g,q_i\}^{\mu\nu\rho} = g^{\mu\nu}q_i^\rho + g^{\nu\rho}q_i^\mu + g^{\mu\rho}q_i^\nu$ and $A_{00}, B_1, \cdots, D_{333}$ are so-called Passarino-Veltman functions (PV-functions) [87]. These functions have been implemented into `LoopTools` [67] for numerical computations.

APPENDIX B: THE COUPLINGS

In this Appendix, we present all the related couplings to the processes under consideration in this paper. We begin with the vector $B-L$ model and show the couplings in the chiral $B-L$ model in the following subsections.

Vector $B-L$ Model

We first derive the coupling of Z to the fermion pair, $Z\bar{f}f$. To illustrate this, we take $Z\bar{q}q$ with quark q in the first generation of matter contents. In detail, the couplings are derived as follows:

$$\mathcal{L}_{Z\bar{q}q} \supset \mathrm{i}\bar{q}_L \not{D} q_L + \mathrm{i}\bar{u}_R \not{D} u_R + \mathrm{i}\bar{d}_R \not{D} d_R \tag{B1}$$

$$
\begin{aligned}
&= -\frac{1}{2}\begin{pmatrix} \bar{u}_L & \bar{d}_L \end{pmatrix}\gamma_\mu Z^\mu \begin{bmatrix} gc_W c_{BL} - (2Q-1)g' s_W c_{BL} & 0 \\ 0 & -gc_W c_{BL} - (2Q+1)g' s_W c_{BL} \end{bmatrix}\begin{pmatrix} u_L \\ d_L \end{pmatrix} \\
&\quad - g' Y_{u_R}(-s_W c_{BL})\bar{u}_R\gamma_\mu Z^\mu u_R - g' Y_{d_R}(-s_W c_{BL})\bar{d}_R\gamma_\mu Z^\mu d_R \\
&\quad - s_{BL}\Big(\frac{g_X Y_X}{\sqrt{1-\kappa^2}} - g' Y_{u_L}\frac{\kappa}{\sqrt{1-\kappa^2}}\Big)\bar{u}_L\gamma_\mu Z^\mu u_L - s_{BL}\Big(\frac{g_X Y_X}{\sqrt{1-\kappa^2}} - g' Y_{d_L}\frac{\kappa}{\sqrt{1-\kappa^2}}\Big)\bar{d}_L\gamma_\mu Z^\mu d_L \\
&\quad - s_{BL}\Big(\frac{g_X Y_X}{\sqrt{1-\kappa^2}} - g' Y_{u_R}\frac{\kappa}{\sqrt{1-\kappa^2}}\Big)\bar{u}_R\gamma_\mu Z^\mu u_R - s_{BL}\Big(\frac{g_X Y_X}{\sqrt{1-\kappa^2}} - g' Y_{d_R}\frac{\kappa}{\sqrt{1-\kappa^2}}\Big)\bar{d}_R\gamma_\mu Z^\mu d_R
\end{aligned} \tag{B2}
$$

$$
\begin{aligned}
&= -\frac{1}{12}\frac{e}{s_W c_W}\bar{u}\gamma_\mu Z^\mu\Big[(1-\gamma_5)(3-6Q_{u_L}s_W^2) - (1+\gamma_5)(6s_W^2 Y_{u_R})\Big]c_{BL}\, u \\
&\quad - \frac{1}{12}\frac{e}{s_W c_W}\bar{d}\gamma_\mu Z^\mu\Big[-(1-\gamma_5)(3+6Q_{d_L}s_W^2) - (1+\gamma_5)(6s_W^2 Y_{d_R})\Big]c_{BL}\, d \\
&\quad - \Big[\frac{g_X Y_X}{\sqrt{1-\kappa^2}} - \frac{g'}{2}[Y_{u_L} + Y_{u_R} + (Y_{u_R} - Y_{u_L})\gamma_5]\frac{\kappa}{\sqrt{1-\kappa^2}}\Big]s_{BL}\bar{u}\gamma_\mu Z^\mu u \\
&\quad - \Big[\frac{g_X Y_X}{\sqrt{1-\kappa^2}} - \frac{g'}{2}[Y_{d_L} + Y_{d_R} + (Y_{d_R} - Y_{d_L})\gamma_5]\frac{\kappa}{\sqrt{1-\kappa^2}}\Big]s_{BL}\bar{d}\gamma_\mu Z^\mu d.
\end{aligned} \tag{B3}
$$

We next calculate the couplings of $Z'\bar{q}q$ as follows:

$$
\mathcal{L}_{Z'\bar{q}q} \supset \mathrm{i}\bar{q}_L \not{D} q_L + \mathrm{i}\bar{u}_R \not{D} u_R + \mathrm{i}\bar{d}_R \not{D} d_R \tag{B4}
$$

$$
\begin{aligned}
&= -\frac{1}{2}\begin{pmatrix} \bar{u}_L & \bar{d}_L \end{pmatrix}\gamma_\mu Z'^\mu \begin{bmatrix} -gc_W s_{BL} + (2Q-1)g' s_W s_{BL} & 0 \\ 0 & gc_W s_{BL} + (2Q+1)g' s_W s_{BL} \end{bmatrix}\begin{pmatrix} u_L \\ d_L \end{pmatrix} \\
&\quad - g' Y_{u_R} s_W s_{BL}\, \bar{u}_R\gamma_\mu Z'^\mu u_R - g' Y_{d_R} s_W s_{BL}\, \bar{d}_R\gamma_\mu Z'^\mu d_R
\end{aligned} \tag{B5}
$$

$$
\begin{aligned}
&\quad - \Big(\frac{g_X Y_X}{\sqrt{1-\kappa^2}} - g' Y_{u_L}\frac{\kappa}{\sqrt{1-\kappa^2}}\Big)c_{BL}\, \bar{u}_L\gamma_\mu Z'^\mu u_L - \Big(\frac{g_X Y_X}{\sqrt{1-\kappa^2}} - g' Y_{d_L}\frac{\kappa}{\sqrt{1-\kappa^2}}\Big)c_{BL}\, \bar{d}_L\gamma_\mu Z'^\mu d_L \\
&\quad - \Big(\frac{g_X Y_X}{\sqrt{1-\kappa^2}} - g' Y_{u_R}\frac{\kappa}{\sqrt{1-\kappa^2}}\Big)c_{BL}\, \bar{u}_R\gamma_\mu Z'^\mu u_R - \Big(\frac{g_X Y_X}{\sqrt{1-\kappa^2}} - g' Y_{d_R}\frac{\kappa}{\sqrt{1-\kappa^2}}\Big)c_{BL}\, \bar{d}_R\gamma_\mu Z'^\mu d_R \\
&= -\frac{1}{12}\frac{e}{s_W c_W}\bar{u}\gamma_\mu Z'^\mu\Big[(1-\gamma_5)(-3+6Q_{u_L}s_W^2) + (1+\gamma_5)6s_W^2 Y_{u_R}\Big]s_{BL} u \\
&\quad - \frac{1}{12}\frac{e}{s_W c_W}\bar{u}\gamma_\mu Z'^\mu\Big[(1-\gamma_5)(3+6Q_{d_L}s_W^2) + (1+\gamma_5)s_W^2 6Y_{d_R}\Big]s_{BL} d \\
&\quad - \Big[\frac{g_X Y_X}{\sqrt{1-\kappa^2}} - \frac{g'}{2}[Y_{u_L} + Y_{u_R} + (Y_{u_R} - Y_{u_L})\gamma_5]\frac{\kappa}{\sqrt{1-\kappa^2}}\Big]c_{BL}\bar{u}\gamma_\mu Z'^\mu u \\
&\quad - \Big[\frac{g_X Y_X}{\sqrt{1-\kappa^2}} - \frac{g'}{2}[Y_{d_L} + Y_{d_R} + (Y_{d_R} - Y_{d_L})\gamma_5]\frac{\kappa}{\sqrt{1-\kappa^2}}\Big]c_{BL}\bar{d}\gamma_\mu Z'^\mu d.
\end{aligned} \tag{B6}
$$

The general couplings of $Z\bar{f}f$ and $Z'\bar{f}f$ with arbitrary fermions f are presented in Table 5.

The components of Higgs kinetic for the vector $B-L$ model can be written as follows:

$$
\begin{aligned}
\mathcal{L}_K \supset (D_\mu\Phi)^\dagger(D_\mu\Phi) \supset{}& \frac{g^2 v_\Phi c_\theta}{2} h W^{\mp,\mu}W^\pm_\mu + \frac{gg' c_w v_\Phi}{2} A^\mu W^\mp_\mu G^\pm + \frac{\mathrm{i}gc_\theta}{2}(\partial^\mu h W^+_\mu G^- - hW^+_\mu\partial^\mu G^- - \partial^\mu h W^-_\mu G^+ + hW^-_\mu\partial^\mu G^+) \\
&+ \frac{\mathrm{i}(gs_W + g' c_W)}{2}(A^\mu G^-\partial_\mu G^+ - A^\mu G^+\partial_\mu G^-)
\end{aligned}
$$

$$
\begin{aligned}
&+\mathrm{i}\Big[\frac{(gc_W-g's_W)}{2}c_{BL}-s_{BL}\frac{g'\kappa}{2\sqrt{1-\kappa^2}}\Big](Z^\mu G^-\partial_\mu G^+-Z^\mu G^+\partial_\mu G^-)+\mathrm{i}\Big[\frac{(g's_W-gc_W)}{2}s_{BL}-c_{BL}\frac{g'\kappa}{2\sqrt{1-\kappa^2}}\Big](Z'_\mu G^-\partial^\mu G^+-Z'_\mu G^+\partial^\mu G^-)\\
&-\frac{gv_\Phi}{2}\Big(g's_Wc_{BL}+s_{BL}\frac{g'\kappa}{\sqrt{1-\kappa^2}}\Big)Z^\mu W^\pm_\mu G^\mp+\frac{gv_\Phi}{2}\Big(g's_Ws_{BL}-c_{BL}\frac{g'\kappa}{\sqrt{1-\kappa^2}}\Big)Z'^\mu W^\pm_\mu G^\mp\\
&+\frac{v_\Phi c_\theta}{2}\Big[(gc_W+g's_W)c_{BL}-s_{BL}g'\frac{\kappa}{\sqrt{1-\kappa^2}}\Big]^2hZ^\mu Z_\mu+\frac{v_\Phi c_\theta}{2}\Big[(gc_W+g's_W)s_{BL}-c_{BL}g'\frac{\kappa}{\sqrt{1-\kappa^2}}\Big)^2hZ'^\mu Z'_\mu\\
&-\frac{v_\Phi c_\theta}{2}\Big[(gc_W+g's_W)c_{BL}+s_{BL}g'\frac{\kappa}{\sqrt{1-\kappa^2}}\Big]\times\Big[(gc_W+g's_W)s_{BL}-c_{BL}g'\frac{\kappa}{\sqrt{1-\kappa^2}}\Big]hZ^\mu Z'_\mu.
\end{aligned}
\tag{B7}
$$

We also have

$$
\mathcal{L}_K\supset(D_\mu\chi)^\dagger(D_\mu\chi)\supset g_X^2Y_X^2v_\chi s_\theta\,hX^\mu X_\mu=g_X^2Y_X^2v_\chi s_\theta\frac{s_{(2BL)}}{1-\kappa^2}hZ^\mu Z'_\mu+g_X^2Y_X^2v_\chi s_\theta\frac{s_{BL}^2}{1-\kappa^2}hZ^\mu Z_\mu+g_X^2Y_X^2v_\chi s_\theta\frac{c_{BL}^2}{1-\kappa^2}hZ'^\mu Z'_\mu. \tag{B8}
$$

Here, we have already used the relation

$$
X^\mu=\frac{1}{\sqrt{1-\kappa^2}}\tilde{X}^\mu=\frac{1}{\sqrt{1-\kappa^2}}(Z^\mu s_{BL}+Z'^\mu c_{BL}). \tag{B9}
$$

The Higgs potential is expanded and we collect the coupling of $2v_\chi s_\theta$

$$
\mathcal{V}(\Phi,\chi)\supset\Big[\lambda_\Phi v_\Phi\Big(c_\theta+\frac{v_\Phi}{v_\chi}s_\theta)+2m_\Phi^2\frac{s_\theta}{v_\chi}\Big]\,hG^+G^- \tag{B10}
$$

We have used the following relations:

$$
\frac{\lambda_\Phi}{2}=\frac{M_{H_2}^2}{4v_\Phi^2}(1-c_{2\theta})+\frac{M_{H_1}^2}{4v_\Phi^2}(1+c_{2\theta}), \tag{B11}
$$

$$
\frac{\lambda_\chi}{2}=\frac{M_{H_1}^2}{4v_\chi^2}(1-c_{2\theta})+\frac{M_{H_2}^2}{4v_\chi^2}(1+c_{2\theta}), \tag{B12}
$$

$$
\lambda_{\Phi\chi}=s_{2\theta}(\frac{M_{H_2}^2-M_{H_1}^2}{2v_\Phi v_\chi}). \tag{B13}
$$

As a result, we arrive at

$$
\begin{aligned}
\lambda_\Phi v_\Phi(c_\theta+\frac{v_\Phi}{v_\chi}s_\theta)+2m_\Phi^2\frac{s_\theta}{v_\chi}&=\lambda_\Phi v_\Phi(c_\theta+\frac{v_\Phi}{v_\chi}s_\theta)-(\lambda_\Phi v_\Phi^2+\lambda_{\Phi\chi}v_\chi^2)\frac{s_\theta}{v_\chi}\\
&=\lambda_\Phi v_\Phi c_\theta-\lambda_{\Phi\chi}v_\chi s_\theta=\frac{M_{H_2}^2}{2v_\Phi}(1-c_{2\theta})c_\theta+\frac{M_{H_1}^2}{2v_\Phi}(1+c_{2\theta})c_\theta-s_{2\theta}(\frac{M_{H_2}^2-M_{H_1}^2}{2v_\Phi})s_\theta\\
&=\frac{M_{H_2}^2}{2v_\Phi}[(1-c_{2\theta})c_\theta-s_{2\theta}s_\theta]+\frac{M_{H_1}^2}{2v_\Phi}[(1+c_{2\theta})c_\theta+s_{2\theta}s_\theta]=\frac{M_{H_2}^2}{2v_\Phi}[2c_\theta s_\theta^2-2c_\theta s_\theta^2]+\frac{M_{H_1}^2}{2v_\Phi}[(1+c_{2\theta})c_\theta+s_{2\theta}s_\theta]\\
&=\frac{M_{H_1}^2}{2v_\Phi}[2c_\theta^2+2{s_\theta}^2]c_\theta=\frac{M_{H_1}^2}{v_\Phi}c_\theta.
\end{aligned}
\tag{B14}
$$

Chiral $B-L$ Model

We are going to calculate all the couplings related to the processes in the chiral $B-L$ model.

The fermion Lagrangian will be expanded as follows:

$$\begin{aligned}\mathcal{L}_{Zff} \supset\ & \bar{u}^i\gamma_\mu\Big[-\frac{1}{4}(1-\gamma_5)(gc_W+(1-2Q_{u_L})g's_W)+\frac{1}{2}(1+\gamma_5)g'c_WY_{u_R}\Big]c'_{BL}\,u^i\,Z^\mu\\ &+\bar{d}^i\gamma_\mu\Big[-\frac{1}{4}(1-\gamma_5)(-gc_W-(2Q_{d_L}+1)g's_W)+\frac{1}{2}(1+\gamma_5)g'c_WY_{d_R})c'_{BL}d^i\,Z^\mu\\ &+s'_{BL}g_XY_X^{u^i}\bar{u}^i\gamma_\mu u^i\,Z^\mu+s'_{BL}g_XY_X^{d^i}\bar{d}^i\gamma_\mu d^i\,Z^\mu+\bar{e}^i\gamma_\mu\Big[\frac{1}{4}(1-\gamma_5)(gc_Wc'_{BL}+(2Q_{e_L}+1)g's_W)\\ &+\frac{1}{2}(1+\gamma_5)g'Y_{e_R}c_W]c'_{BL}e^i\,Z^\mu+s'_{BL}g_XY_X^{e^i}\bar{e}^i\gamma_\mu e^i\,Z^\mu.\end{aligned} \tag{B15}$$

$$\begin{aligned}\mathcal{L}_{Z'ff} \supset\ & \bar{u}^i\gamma_\mu\Big[\frac{-1}{4}(1-\gamma_5)(gc_W+(1-2Q_{u_L})g's_W)+\frac{1}{2}(1+\gamma_5)g's_WY_{u_R}\Big]s'_{BL}u^i\,Z'^\mu\\ &+\bar{d}^i\gamma_\mu\Big[\frac{-1}{4}(1-\gamma_5)(-gc_W-(2Q_{d_L}+1)g's_W)+\frac{1}{2}(1+\gamma_5)g's_WY_{d_R}\Big]s'_{BL}d^i\,Z'^\mu\\ &-c'_{BL}g_XY_X^{u^i}\bar{u}^i\gamma_\mu u^i\,Z'^\mu-c'_{BL}g_XY_X^{d^i}\bar{d}^i\gamma_\mu d^i\,Z'^\mu+\bar{e}^i\gamma_\mu\Big[\frac{1}{4}(1-\gamma_5)(gc_Ws'_{BL}+(2Q_{e_L}+1)g's_W)\\ &+\frac{1}{2}(1+\gamma_5)g'Y_{e_R}s_W\Big]s'_{BL}e^i\,Z'^\mu-c'_{BL}g_XY_X^{e^i}\bar{e}^i\gamma_\mu e^i\,Z'^\mu.\end{aligned} \tag{B16}$$

The general formulas for the couplings of $Z\,(Z')$ with the fermion-pair are given in Table 10.

The components of Higgs kinetic for the chiral $B-L$ model can be written as follows:

$$\mathcal{L}_K \supset (D_\mu\Phi)^\dagger(D_\mu\Phi)+(D_\mu\varphi)^\dagger(D_\mu\varphi) \tag{B17}$$

$$\begin{aligned}\supset\ & \frac{g^2}{2}(v_\Phi c_{13}c_{12}-v_\varphi c_{13}s_{12})\,hW^{\pm,\mu}W_\mu^\mp-\frac{gg's_W}{2}(c_\alpha v_\Phi+s_\alpha v_\varphi)s'_{BL}\,Z'^\mu W_\mu^\pm G^\mp\\ &-\frac{gg's_W}{2}(c_\alpha v_\Phi+s_\alpha v_\varphi)c'_{BL}\,Z^\mu W_\mu^\pm G^\mp+\frac{\mathrm{i}(gs_W+g'c_W)}{2}\,(A^\mu G^-\partial_\mu G^+-A^\mu G^+\partial_\mu G^-)\\ &+\frac{\mathrm{i}(gc_W-g's_W)c'_{BL}}{2}\,(Z^\mu G^-\partial_\mu G^+-Z^\mu G^+\partial_\mu G^-)+\frac{\mathrm{i}(gc_W-g's_W)s'_{BL}}{2}\,(Z'^\mu G^-\partial_\mu G^+-Z'^\mu G^+\partial_\mu G^-)\\ &+\frac{\mathrm{i}(gs_W+g'c_W)}{2}\,(A^\mu H^-\partial_\mu H^+-A^\mu H^+\partial_\mu H^-)+\frac{\mathrm{i}(gc_W-g'c_W)c'_{BL}}{2}\,(Z^\mu H^-\partial_\mu H^+-Z^\mu H^+\partial_\mu H^-)\\ &+\frac{\mathrm{i}(gc_W-g's_W)s'_{BL}}{2}\,(Z'^\mu H^-\partial_\mu H^+-Z'^\mu H^+\partial_\mu H^-)+\frac{(gc_W+g's_W)^2(v_\Phi c_{13}c_{12}-v_\varphi c_{13}s_{12})c'^2_{BL}}{4}\,hZ^\mu Z_\mu\\ &+\frac{(gc_W+g's_W)^2(v_\Phi c_{13}c_{12}-v_\varphi c_{13}s_{12})s'^2_{BL}}{4}\,hZ'^\mu Z'_\mu+\frac{(gc_W+g's_W)^2(v_\Phi c_{12}-v_\varphi s_{12})c_{13}s'_{BL}c'_{BL}}{2}\,hZ^\mu Z'_\mu\\ &+\frac{\mathrm{i}gc_{13}(c_{12}c_\alpha-s_{12}s_\alpha)}{2}\,(hW_\mu^-\partial^\mu G^+-hW_\mu^+\partial^\mu G^--\partial^\mu hW_\mu^-G^++\partial^\mu hW_\mu^+G^-).\end{aligned} \tag{B18}$$

$$\begin{aligned}\mathcal{L}_K &\supset (D_\mu\varphi)^\dagger(D_\mu\varphi)\supset g_X^2Y_X^2X^\mu X_\mu[G_2^\pm G_2^\mp+\frac{1}{2}(v_\varphi+R_2+\mathrm{i}I_2)(v_\varphi+R_2-\mathrm{i}I_2)]\\ &\supset\frac{1}{2}g_X^2Y_X^2v_\sigma(-s'_{BL}Z^\mu+c'_{BL}Z'^\mu)(-s'_{BL}Z_\mu+c'_{BL}Z'_\mu)(v_\varphi+R_2)^2\supset g_X^2Y_X^2v_\sigma(-s'_{BL}Z^\mu+c'_{BL}Z'^\mu)(-s'_{BL}Z_\mu+c'_{BL}Z'_\mu)v_\varphi(-c_{13}s_{12})h\\ &=-g_X^2Y_X^2v_\sigma c_{13}s_{12}h(s'^2_{BL}Z^\mu Z_\mu+c'^2_{BL}Z'^\mu Z'_\mu-s'_{BL}c'_{BL}Z^\mu Z'_\mu-s'_{BL}c'_{BL}\,Z'_\mu Z^\mu)\\ &=-g_X^2Y_X^2v_\sigma c_{13}s_{12}s'^2_{BL}\,hZ^\mu Z_\mu-g_X^2Y_X^2v_\sigma c_{13}s_{12}c'^2_{BL}\,hZ'^\mu Z'_\mu+2g_X^2Y_X^2v_\sigma c_{13}s_{12}s'_{BL}c'_{BL}\,hZ^\mu Z'_\mu.\end{aligned} \tag{B19}$$

Another term in the kinematic part of the Higgs sector is expressed as

$$\begin{aligned}\mathcal{L}_K &\supset (D_\mu\sigma)^\dagger(D_\mu\sigma) \supset \frac{1}{2}g_X^2Y_X^2X^\mu X_\mu(2v_\sigma)R_3 = g_X^2Y_X^2v_\sigma(-s'_{BL}Z^\mu + c'_{BL}Z'^\mu)(-s'_{BL}Z_\mu + c'_{BL}Z'_\mu)s_{13}h \\ &= g_X^2Y_X^2v_\sigma s_{13}h(s'^2_{BL}Z^\mu Z_\mu + c'^2_{BL}Z'^\mu Z'_\mu - s'_{BL}c'_{BL}Z^\mu Z'_\mu - s'_{BL}c'_{BL}Z'^\mu Z_\mu) \\ &= g_X^2Y_X^2v_\sigma s_{13}s'^2_{BL}\,hZ^\mu Z_\mu + g_X^2Y_X^2v_\sigma s_{13}c'^2_{BL}\,hZ'^\mu Z'_\mu - 2g_X^2Y_X^2v_\sigma s_{13}s'_{BL}c'_{BL}\,hZ^\mu Z'_\mu. \end{aligned} \tag{B20}$$

The Higgs potential is

$$\begin{aligned}\mathcal{V}(\Phi,\varphi,\sigma,\chi_d) \supset &\Big\{\lambda_\Phi v_\Phi c_{13}c_{12}c_\alpha^2 - \lambda_\varphi v_\varphi c_{13}s_{12}s_\alpha^2 + \frac{\mu}{\sqrt{2}}s_{13}s_\alpha c_\alpha + \frac{\mu}{\sqrt{2}}s_{13}s_\alpha c_\alpha \\ &- \lambda_{\Phi\sigma}v_\sigma c_\alpha^2 s_{13} - \lambda_{\varphi\sigma}v_\sigma s_\alpha^2 s_{13} + \lambda_{\Phi\varphi_1}[-c_{13}s_{12}c_\alpha^2 v_\varphi + c_{13}c_{12}s_\alpha^2 v_\Phi] \\ &+ \lambda_{\Phi\varphi_2}(-v_\Phi c_{13}s_{12} + v_\varphi c_{13}c_{12})s_\alpha c_\alpha\Big\}\, G^-G^+h \\ &+ \Big\{\lambda_\Phi v_\Phi c_{13}c_{12}s_\alpha^2 - \lambda_\varphi v_\varphi c_{13}s_{12}c_\alpha^2 - \frac{\mu}{\sqrt{2}}s_{13}s_\alpha c_\alpha - \frac{\mu}{\sqrt{2}}s_{13}s_\alpha c_\alpha \\ &- \lambda_{\Phi\sigma}v_\sigma s_\alpha^2 s_{13} - \lambda_{\varphi\sigma}v_\sigma c_\alpha^2 s_{13} + \lambda_{\Phi\varphi_1}[-c_{13}s_{12}s_\alpha^2 v_\varphi + c_{13}c_{12}c_\alpha^2 v_\Phi] \\ &- \lambda_{\Phi\varphi_2}(-v_\Phi c_{13}s_{12} + v_\varphi c_{13}c_{12})s_\alpha c_\alpha\Big\}H^-H^+h. \end{aligned} \tag{B21}$$

The Yukawa Lagrangian is expanded as follows;

$$\begin{aligned}-\mathcal{L}_Y &= Y_e\bar{L}\Phi e_R + Y_u\bar{Q}\tilde{\Phi}u_R + Y_e\bar{Q}\Phi d_R + Y_\nu\bar{L}\tilde{\varphi}\nu_R + h.c \\ &\supset Y_\nu\begin{pmatrix}\bar{\nu}_L & \bar{e}_L\end{pmatrix}\begin{pmatrix}\frac{1}{\sqrt{2}}(v_\varphi + R_2 + \mathrm{i}I_2) & \\ & G_2^\pm\end{pmatrix}\nu_R + Y_\nu\bar{\nu}_R\begin{pmatrix}\frac{1}{\sqrt{2}}(v_\varphi + R_2 + iI_2) & G_2^\mp\end{pmatrix}\begin{pmatrix}\nu_L \\ e_L\end{pmatrix} \\ &= \frac{Y_\nu v_\varphi}{\sqrt{2}}\bar{\nu}_L\nu_R + \frac{Y_\nu v_\varphi}{\sqrt{2}}\bar{\nu}_R\nu_L + \frac{s_\alpha Y_\nu(1+\gamma_5)}{2}\bar{e}G^\pm\nu_R + \frac{c_\alpha Y_\nu(1+\gamma_5)}{2}\bar{e}H^\pm\nu_R \\ &\quad + \frac{s_\alpha Y_\nu(1-\gamma_5)}{2}\bar{\nu}_R G^\mp e + \frac{c_\alpha Y_\nu(1-\gamma_5)}{2}\bar{\nu}_R H^\mp e \end{aligned} \tag{B22}$$

In the limits of $c_{13}, c_{23} \to 1$, the mixing angle between $H_1 = h$ and H_2 is considered to be $c_{\widehat{12}}$; then, the coupling of hH^+H^- takes the form of

$$g_{hH^\pm H^\mp} = \lambda_\Phi v_\Phi c_{\widehat{12}}s_\alpha^2 - \lambda_\phi v_\phi s_{\widehat{12}}c_\alpha^2 + \lambda_{\Phi\phi_1}(-s_{\widehat{12}}s_\alpha^2 v_\phi + c_{\widehat{12}}c_\alpha^2 v_\Phi) - \lambda_{\Phi\phi_2}(-v_\Phi s_{\widehat{12}} + v_\phi c_{\widehat{12}})s_\alpha c_\alpha \tag{B23}$$

$$\begin{aligned}&= \frac{c_{2(\widehat{12})}}{v_\Phi}[M_h^2(c_{\widehat{12}}^2 + t_{2(\widehat{12})}s_{\widehat{12}}c_{\widehat{12}}) - M_H^2(s_{\widehat{12}}^2 - t_{2(\widehat{12})}s_{\widehat{12}}c_{\widehat{12}})]c_{\widehat{12}}s_\alpha^2 - \frac{\mu v_\phi v_\sigma}{\sqrt{2}v_\Phi^2}c_{\widehat{12}}s_\alpha^2 \\ &\quad + \frac{c_{2(\widehat{12})}}{v_\phi}[M_h^2(s_{\widehat{12}}^2 - t_{2(\widehat{12})}s_{\widehat{12}}c_{\widehat{12}}) - M_H^2(c_{\widehat{12}}^2 + t_{2(\widehat{12})}s_{\widehat{12}}c_{\widehat{12}})]s_{\widehat{12}}c_\alpha^2 + \frac{\mu v_\Phi v_\sigma}{\sqrt{2}v_\phi^2}s_{\widehat{12}}c_\alpha^2 \\ &\quad + [(M_H^2 - M_h^2)\frac{s_{2(\widehat{12})}}{2v_\Phi v_\phi} - \frac{\mu v_\sigma}{\sqrt{2}v_\Phi v_\phi} + \frac{2M_{H^\pm}^2}{v^2}](-s_{\widehat{12}}s_\alpha^2 v_\phi + c_{\widehat{12}}c_\alpha^2 v_\Phi) \\ &\quad - (\frac{\sqrt{2}\mu v_\sigma}{v_\Phi v_\phi} - \frac{2M_{H^\pm}^2}{v^2})(-v_\Phi s_{\widehat{12}} + v_\phi c_{\widehat{12}})s_\alpha c_\alpha \end{aligned} \tag{B24}$$

$$= \frac{1}{v}[\frac{\sqrt{2}\mu v_\sigma}{s_\alpha c_\alpha}\cot(2\alpha)s_{\alpha+\widehat{12}} + \frac{M_h^2}{s_\alpha c_\alpha}s_{\alpha-\widehat{12}}] + \frac{1}{v}(2M_{H^\pm}^2 - \frac{\sqrt{2}\mu v_\sigma}{s_\alpha c_\alpha} - M_h^2)c_{\alpha+\widehat{12}}. \tag{B25}$$

Here, we have applied the following relations:

$$M_h^2 = \lambda_\Phi v_\Phi^2 c_{\widehat{12}}^2 + \frac{\mu v_\phi v_\sigma}{\sqrt{2} v_\Phi} c_{\widehat{12}}^2 - (\lambda_{12} v_\Phi v_\phi - \frac{\mu v_\sigma}{\sqrt{2}}) s_{2(\widehat{12})} + \lambda_\phi v_\phi^2 s_{\widehat{12}}^2 + \frac{\mu v_\Phi v_\sigma}{\sqrt{2} v_\phi} s_{\widehat{12}}^2, \tag{B26}$$

$$M_H^2 = \lambda_\Phi v_\Phi^2 s_{\widehat{12}}^2 + \frac{\mu v_\phi v_\sigma}{\sqrt{2} v_\Phi} s_{\widehat{12}}^2 + (\lambda_{12} v_\Phi v_\phi - \frac{\mu v_\sigma}{\sqrt{2}}) s_{2(\widehat{12})} + \lambda_\phi v_\phi^2 c_{\widehat{12}}^2 + \frac{\mu v_\Phi v_\sigma}{\sqrt{2} v_\phi} c_{\widehat{12}}^2 \tag{B27}$$

and

$$-v_\phi^2 \lambda_\phi = c_{2(\widehat{12})} [M_h^2 (s_{\widehat{12}}^2 - t_{2(\widehat{12})} s_{\widehat{12}} c_{\widehat{12}}) - M_H^2 (c_{\widehat{12}}^2 + t_{2(\widehat{12})} s_{\widehat{12}} c_{\widehat{12}})] + \frac{\mu v_\Phi v_\sigma}{\sqrt{2} v_\phi}, \tag{B28}$$

$$v_\Phi^2 \lambda_\Phi = c_{2(\widehat{12})} [M_h^2 (c_{\widehat{12}}^2 + t_{2(\widehat{12})} s_{\widehat{12}} c_{\widehat{12}}) - M_H^2 (s_{\widehat{12}}^2 - t_{2(\widehat{12})} s_{\widehat{12}} c_{\widehat{12}})] - \frac{\mu v_\phi v_\sigma}{\sqrt{2} v_\Phi}, \tag{B29}$$

$$\lambda_{\Phi\phi_1} = [M_H^2 - M_h^2] \frac{s_{2(\widehat{12})}}{2 v_\Phi v_\phi} - \frac{\mu v_\sigma}{\sqrt{2} v_\Phi v_\phi} + \frac{2 M_{H^\pm}^2}{v^2}. \tag{B30}$$

References

[1] A. Liss *et al.* (ATLAS Collaboration), arXiv: 1307.7292 [hep-ex]
[2] CMS Collaboration, arXiv: 1307.7135 [hep-ex]
[3] H. Baer, T. Barklow, K. Fujii *et al.*, arXiv: 1306.6352 [hep-ph]
[4] G. Aad *et al.*, JHEP **08**, 045 (2016), arXiv:1606.02266[hep-ex]
[5] G. Aad *et al.*, Phys. Rev. D **101**(1), 012002 (2020), arXiv:1909.02845[hep-ex]
[6] V. Khachatryan *et al.*, Eur. Phys. J. C **75**(5), 212 (2015), arXiv:1412.8662[hep-ex]
[7] G. Aad *et al.*, Eur. Phys. J. C **76**(1), 6 (2016), arXiv:1507.04548[hep-ex]
[8] A. M. Sirunyan *et al.*, JHEP **07**, 027 (2021), arXiv:2103.06956[hep-ex]
[9] V. M. Abazov *et al.*, Phys. Lett. B **671**, 349 (2009), arXiv:0806.0611[hep-ex]
[10] S. Chatrchyan *et al.*, Phys. Lett. B **726**, 587 (2013), arXiv:1307.5515[hep-ex]
[11] M. Aaboud *et al.*, JHEP **10**, 112 (2017), arXiv:1708.00212[hep-ex]
[12] G. Aad *et al.*, Phys. Lett. B **809**, 135754 (2020), arXiv:2005.05382[hep-ex]
[13] V. Khachatryan *et al.*, Phys. Lett. B **753**, 341 (2016), arXiv:1507.03031[hep-ex]
[14] A. M. Sirunyan *et al.*, JHEP **09**, 148 (2018), arXiv:1712.03143[hep-ex]
[15] A. M. Sirunyan *et al.*, JHEP **11**, 152 (2018), arXiv:1806.05996[hep-ex]
[16] G. Aad *et al.*, Phys. Lett. B **819**, 136412 (2021), arXiv:2103.10322[hep-ex]
[17] L. B. Chen, C. F. Qiao, and R. L. Zhu, Phys. Lett. B **726**, 306 (2013), [Erratum: Phys. Lett. B 808, 135629 (2020)], arXiv: 1211.6058[hep-ph]
[18] J. S. Gainer, W. Y. Keung, I. Low *et al.*, Phys. Rev. D **86**, 033010 (2012), arXiv:1112.1405[hep-ph]
[19] A. Y. Korchin and V. A. Kovalchuk, Eur. Phys. J. C **74**(11), 3141 (2014), arXiv:1408.0342[hep-ph]
[20] A. Abbasabadi and W. W. Repko, Phys. Rev. D **62**, 054025 (2000), arXiv:hep-ph/0004167[hep-ph]
[21] D. A. Dicus and W. W. Repko, Phys. Rev. D **87**(7), 077301 (2013), arXiv:1302.2159[hep-ph]
[22] Y. Sun, H. R. Chang, and D. N. Gao, JHEP **05**, 061 (2013), arXiv:1303.2230[hep-ph]
[23] G. Passarino, Phys. Lett. B **727**, 424 (2013), arXiv:1308.0422[hep-ph]
[24] D. A. Dicus, C. Kao, and W. W. Repko, Phys. Rev. D **89**(3), 033013 (2014), arXiv:1310.4380[hep-ph]
[25] A. Kachanovich, U. Nierste, and I. Nišandžić, Phys. Rev. D **101**(7), 073003 (2020), arXiv:2001.06516[hep-ph]
[26] A. Kachanovich, U. Nierste, and I. Nišandžić, Phys. Rev. D **105**(1), 013007 (2022), arXiv:2109.04426[hep-ph]
[27] I. Ahmed, U. Hasan, S. Iqbal *et al.*, arXiv: 2309.07448 [hep-ph]
[28] C. S. Li, C. F. Qiao, and S. H. Zhu, Phys. Rev. D **57**, 6928 (1998), arXiv:hep-ph/9801334[hep-ph]
[29] K. Sasaki and T. Uematsu, Phys. Lett. B **781**, 290 (2018), arXiv:1712.00197[hep-ph]
[30] K. H. Phan, L. Hue, and D. T. Tran, PTEP **2021**(10), 103B (2021), arXiv:2106.14466[hep-ph]
[31] V. Van On, D. T. Tran, C. L. Nguyen *et al.*, Eur. Phys. J. C **82**(3), 277 (2022), arXiv:2111.07708[hep-ph]

[32] L. T. Hue, D. T. Tran, T. H. Nguyen *et al.*, PTEP **2023**(8), 083B (2023), arXiv:2305.04002[hep-ph]
[33] S. Mandal, H. Prajapati, and R. Srivastava, arXiv: 2301.01522 [hep-ph]
[34] L. Basso, A. Belyaev, S. Moretti, and C. H. Shepherd-Themistocleous, Phys. Rev. D **80**, 055030 (2009), arXiv:0812.4313[hep-ph]
[35] L. Basso, A. Belyaev, S. Moretti *et al.*, JHEP **10**, 006 (2009), arXiv:0903.4777[hep-ph]
[36] L. Basso, A. Belyaev, S. Moretti *et al.*, Phys. Rev. D **81**, 095018 (2010), arXiv:1002.1939[hep-ph]
[37] L. Basso, A. Belyaev, S. Moretti *et al.*, Eur. Phys. J. C **71**, 1613 (2011), arXiv:1002.3586[hep-ph]
[38] L. Basso, S. Moretti, and G. M. Pruna, Phys. Rev. D **82**, 055018 (2010), arXiv:1004.3039[hep-ph]
[39] L. Basso, S. Moretti, and G. M. Pruna, J. Phys. G **39**, 025004 (2012), arXiv:1009.4164[hep-ph]
[40] L. Basso, S. Moretti, and G. M. Pruna, Phys. Rev. D **83**, 055014 (2011), arXiv:1011.2612[hep-ph]
[41] L. Basso, S. Moretti, and G. M. Pruna, Eur. Phys. J. C **71**, 1724 (2011), arXiv:1012.0167[hep-ph]
[42] L. Basso, S. Moretti, and G. M. Pruna, JHEP **08**, 122 (2011), arXiv:1106.4762[hep-ph]
[43] J. C. Pati and A. Salam, Phys. Rev. D **10**, 275 (1975), [Erratum: Phys. Rev. D 11, 703 (1997)]
[44] R. N. Mohapatra and J. C. Pati, Phys. Rev. D **11**, 2558 (1975)
[45] G. Senjanovic and R. N. Mohapatra, Phys. Rev. D **12**, 1502 (1975)
[46] M. Singer, J. W. F. Valle, and J. Schechter, Phys. Rev. D **22**, 738 (1980)
[47] J. W. F. Valle and M. Singer, Phys. Rev. D **28**, 540 (1983)
[48] F. Pisano and V. Pleitez, Phys. Rev. D **46**, 410 (1992)
[49] P. H. Frampton, Phys. Rev. Lett **69**, 2889 (1992)
[50] R. A. Diaz, R. Martinez, and F. Ochoa, Phys. Rev. D **72**, 035018 (2005)
[51] R. M. Fonseca and M. Hirsch, JHEP **08**, 003 (2016)
[52] R. Foot, H. N. Long, and T. A. Tran, Phys. Rev. D **50**(1), R34 (1994)
[53] L. A. Sanchez, F. A. Perez, and W. A. Ponce, Eur. Phys. J. C **35**, 259 (2004), arXiv:hep-ph/0404005[hep-ph]
[54] W. A. Ponce and L. A. Sanchez, Mod. Phys. Lett. A **22**, 435 (2007), arXiv:hep-ph/0607175[hep-ph]
[55] R. Fayyazuddin, Eur. Phys. J. C **56**, 389 (2008), arXiv:0803.4267[hep-ph]
[56] A. Jaramillo and L. A. Sanchez, Phys. Rev. D **84**, 115001 (2011), arXiv:1110.3363[hep-ph]
[57] H. N. Long, L. T. Hue, and D. V. Loi, Phys. Rev. D **94**(1), 015007 (2016), arXiv:1605.07835[hep-ph]
[58] A. Abbasabadi, D. Bowser-Chao, D. A. Dicus *et al.*, Phys. Rev. D **52**, 3919 (1995), arXiv:hep-ph/9507463[hep-ph]
[59] A. Djouadi, V. Driesen, W. Hollik *et al.*, Nucl. Phys. B **491**, 68 (1997), arXiv:hep-ph/9609420[hep-ph]
[60] A. Abbasabadi, D. Bowser-Chao, D. A. Dicus *et al.*, Phys. Rev. D **58**, 057301 (1998), arXiv:hep-ph/9706335[hep-ph]
[61] A. Arhrib, R. Benbrik, and T. C. Yuan, Eur. Phys. J. C **74**, 2892 (2014), arXiv:1401.6698[hep-ph]
[62] L. Rahili, A. Arhrib, and R. Benbrik, Eur. Phys. J. C **79**(11), 940 (2019), arXiv:1909.07793[hep-ph]
[63] S. Kanemura, K. Mawatari, and K. Sakurai, Phys. Rev. D **99**(3), 035023 (2019), arXiv:1808.10268[hep-ph]
[64] M. Demirci, Phys. Rev. D **100**(7), 075006 (2019), arXiv:1905.09363[hep-ph]
[65] T. Hahn, Comput. Phys. Commun. **140**, 418 (2001), arXiv:hep-ph/0012260[hep-ph]
[66] R. Mertig, M. Bohm, and A. Denner, Comput. Phys. Commun. **64**, 345 (1991)
[67] T. Hahn and M. Perez-Victoria, Comput. Phys. Commun. **118**, 153 (1999), arXiv:hep-ph/9807565[hep-ph]
[68] F. Deppisch, S. Kulkarni, and W. Liu, Phys. Rev. D **100**(3), 035005 (2019), arXiv:1905.11889[hep-ph]
[69] M. Carena, A. Daleo, B. A. Dobrescu *et al.*, Phys. Rev. D **70**, 093009 (2004), arXiv:hep-ph/0408098[hep-ph]
[70] G. Cacciapaglia, C. Csaki, G. Marandella *et al.*, Phys. Rev. D **74**, 033011 (2006), arXiv:hep-ph/0604111[hep-ph]
[71] ALEPH Collaboration, DELPHI Collaboration, L3 Collaboration, OPAL Collaboration, the LEP Electroweak Working Group, the SLD Electroweak, Heavy Flavour Groups, arXiv: hep-ex/0312023
[72] G. Aad *et al.*, Phys. Lett. B **796**, 68 (2019), arXiv:1903.06248[hep-ex]
[73] A. M. Sirunyan *et al.*, Phys. Lett. B **798**, 134952 (2019), arXiv:1906.00057[hep-ex]
[74] P. Bechtle, S. Heinemeyer, O. Stal *et al.*, Eur. Phys. J. C **75**(9), 421 (2015), arXiv:1507.06706[hep-ph]
[75] T. Robens and T. Stefaniak, Eur. Phys. J. C **76**(5), 268 (2016), arXiv:1601.07880[hep-ph]
[76] G. Chalons, D. Lopez-Val, T. Robens *et al.*, PoS ICHEP **2016**, 1180 (2016), arXiv:1611.03007[hep-ph]
[77] A. Ilnicka, T. Robens, and T. Stefaniak, Mod. Phys. Lett. A **33**, 1830007 (2018)
[78] O. Adriani *et al.*, Phys. Lett. B **295**, 371 (1992)
[79] P. Abreu *et al.* (DELPHI Collaboration), Z. Phys. C **74**, 57 (1997), [Erratum: Z. Phys. C 75, 580 (1997)]
[80] S. Chatrchyan, *et al*, Phys. Lett. B **717**, 109 (2012), arXiv:1207.6079[hep-ex]
[81] [ATLAS], ATLAS-CONF-2012-139.
[82] V. Khachatryan, *et al*, Phys. Lett. B **748**, 144 (2015), arXiv:1501.05566[hep-ex]
[83] A. M. Sirunyan, *et al*, Phys. Rev. Lett. **120**(22), 221801 (2018), arXiv:1802.02965[hep-ex]
[84] A. M. Sirunyan, *et al*, JHEP **01**, 122 (2019), arXiv:1806.10905[hep-ex]
[85] A. M. Sirunyan, *et al*, Phys. Rev. Lett. **119**(22), 221802 (2017), arXiv:1708.07962[hep-ex]
[86] Y. Aoki, K. Fujii, S. Jung *et al.*, arXiv: 1902.06029 [hep-ex]
[87] A. Denner and S. Dittmaier, Nucl. Phys. B **734**, 62 (2006)